Functional interaction between transcription factor Sfp1 and the NuA4 complex in response to nutrient availability

Ke Xu[1], Charles Joly Beauparlant[2], Stéphanie Bianco[2], Valérie Côté[1], Lara Hermann[2], Arnaud Droit[2], Michael Downey[3], Amine Nourani[1]* and Jacques Côté[1]*

1. St-Patrick Research Group in Basic Oncology, Oncology Division of CHU de Québec-Université Laval Research Center, Laval University Cancer Research Center, Quebec City, QC, G1R 3S3, Canada.

2. Computational Biology Laboratory, CHU de Québec-Université Laval Research Center, Québec City, Québec, G1V 4G2, Canada.

3. Ottawa Institute of Systems Biology, Department of Cellular and Molecular Medicine, University of Ottawa, Ottawa, Ontario, K1H 8M5, Canada.

***correspondance: amine.nourani@crchudequebec.ulaval.ca; jacques.cote@crchudequebec.ulaval.ca;**

Running title : Sfp1 and NuA4 interaction regulates ribosome biogenesis

Abstract

Ribosome biogenesis is a crucial process requiring enormous transcriptional output. In budding yeast, the expression of 138 ribosomal protein (RP) genes and over 200 ribosome biogenesis (RiBi) genes is regulated by and intricate network of factors, including the nutrient-sensitive transcription activator Sfp1 and the NuA4 coactivator/acetyltransferase complex. Nutrient starvation or inhibition of TORC1 by rapamycin leads to repression of RP and RiBi genes, in part through blocking Sfp1 nuclear localization and NuA4-dependent chromatin acetylation. Here, we demonstrate that Sfp1 physically interacts with NuA4 in a TORC1-independent manner. Our results indicate that Sfp1, along with NuA4, regulate transcription of RiBi and RP genes via distinct mechanisms depending on promoter architectures. Sfp1 promotes NuA4-dependent histone acetylation at the promoter of RiBi and RP genes without affecting NuA4 recruitment. In contrast, NuA4 does impact Sfp1 binding but specifically at two classes of RP genes. Importantly, we found that NuA4 acetylates Sfp1 at lysines 655 and lysine 657, regulating its function. Cells expressing Sfp1 with acetyl-mimicking mutations exhibit increased expression of RiBi genes while RP genes remain stable. However, the same mutants lead to the loss of Sfp1 binding/activity at RiBi genes when cells are under non-optimal growth conditions. Mimicking constitutive acetylation of Sfp1 also limits the transcriptional burst of RP genes upon addition of glucose. Altogether, these results draw an intricate functional relationship between Sfp1 and NuA4 to control ribosome biogenesis, fine-tuning transcription output in different growth conditions.

Keywords: ribosome biogenesis, Sfp1, NuA4, acetylation, ribosomal proteins, carbon source, chromatin, transcription, yeast

Introduction

Cells have evolved intricate regulatory networks to adapt their physiology to environmental changes [1]. In budding yeast, the Target of Rapamycin Complex 1 (TORC1) kinase plays a central role in sensing external cues and transmitting signals to regulate cell growth and metabolism in response to nutrient availability and stress [2]. Among the many physiological processes regulated by TORC1, the formation of functional ribosomes stands out as one of the most energy-intensive activities. Yeast ribosomes contain 79 different ribosomal proteins (RP) encoded by 139 RP genes. More than 200 ribosome biogenesis (RiBi) regulons are implicated in ribosome assembly to enable accurate construction and function [3]. To limit unnecessary energy expenditure, the expression of RP and RiBi genes must be tightly controlled at the transcriptional level, which involves sets of activators and coactivators [4, 5][6]. Despite sharing common transcription factors (TFs) with RP genes and showing similar transcriptional responses to nutrient perturbations, RiBi gene promoters are often enriched with the so-called RRPE and PAC motifs and can exhibit distinct regulation [7].

Sfp1 is a zinc finger transcriptional activator that plays a pivotal role in orchestrating the complex expression of RP and RiBi genes in response to nutrient fluctuations [6, 8]. Under optimal growth conditions, TOR kinase phosphorylates Sfp1, promoting its nuclear localization, where it collaborates with various TFs and coactivators to promote RP and RiBi gene expression [9]. However, nutrient starvation or treatment with rapamycin (TORC1 inhibitor) triggers the translocation of Sfp1 to the cytoplasm, resulting in RiBi and RP repression [10]. Coactivators are often recruited by TFs to specific genes to modify chromatin structure, creating a permissive state for transcription. Among the coactivators implicated in RP and RiBi gene activation,

histone acetyltransferase (HAT) complexes SAGA and NuA4 are recruited to the promoter region to acetylate nucleosomes and facilitate transcription [11-13][14, 15]. While SAGA acetylates histones H3 and H2B, NuA4 targets H4 and H2A and both complexes can be recruited through similar mechanisms [16, 17]. NuA4 is a 13-subunit complex that contains the only essential HAT in *Saccharomyces cerevisiae*, Esa1, required for the vast majority of H4, H2A and variant Htz1 acetylation in chromatin [18-21]. We and others previously revealed the extensive binding of NuA4 at RP gene promoters, with its association seeming to be regulated by TORC1 signalling pathway [13, 22-24]. Esa1 positively regulates RP transcription, and its recruitment is correlated with nutrient availabilities. Together, these observations raise the question of a possible functional interaction between Sfp1 and NuA4 to regulate RP and RiBi gene expression.

To test this hypothesis and understand how these two factors may interact functionally, we undertook molecular and global approaches in budding yeast. We show that Sfp1 physically interacts with NuA4 in a TORC1-independent manner. Depletion of Sfp1 results in reduced H3 and H4 acetylation at RiBi and RP promoters, even though NuA4 binding is not affected at these locations. Conversely, loss of NuA4-dependent histone acetylation through Esa1 depletion affects Sfp1 recruitment at specific RP gene promoters. Interestingly, Sfp1 lysine 655 and lysine 657 are acetylated in an Esa1-dependent manner. When nutrients are available, mimicking constitutive Sfp1 acetylation leads to increased occupancy and activity at RiBi genes, whereas no significant changes are observed at RP genes. Noteworthy, cells expressing acetyl-mimicking Sfp1 are more sensitive to nutrient deficiency or TORC1 inhibition, likely reflecting misguided signaling. This implies that, in addition to histone acetylation, NuA4 regulates RP/RiBi gene

expression by modulating the transcriptional function of Sfp1 through non-histone acetylation, in response to nutrient availability.

Results

NuA4 interacts with Sfp1 *in vivo* and *in vitro*

NuA4 and Sfp1 bind to ribosomal protein genes regulating their expression in response to stress and nutrient perturbations [13, 15, 24-28]. However, it is still unknown whether NuA4 and Sfp1 interact physically and functionally at their mutual target genes. To answer this question, we affinity purified Sfp1-TAP fusion protein, expressed from the endogenous *SFP1* locus, and identified interacting proteins by western blotting. As a control, the NuA4 complex from an Epl1-TAP expressing strain was purified in parallel. As shown in Fig 1A, we detected the protein Tra1 in the Sfp1 purified fraction, confirming previous studies [9, 26]. Tra1 is an essential component of both SAGA and NuA4 histone acetyltransferase complexes. It is the recruitment interface for different transcription factors [16]. To specifically ask if Sfp1 interacts with NuA4, we probed for Eaf1, a NuA4-specific subunit [29]. As shown in Fig 1B, Eaf1 as well as Arp4, another NuA4 subunit, were detected in both Sfp1-TAP and Epl1-TAP purified fractions, indicating that Sfp1 interacts physically with NuA4 *in vivo*. We further confirmed the interaction by immunoprecipitation using whole cell extracts of cells expressing Flag-tagged Epl1 and Sfp1-myc (Fig 1C, upper panels). Importantly, TORC1 inhibition with rapamycin does not affect the detected NuA4-Sfp1 interaction (Fig 1C, lower panels). To determine if the physical interaction between Sfp1 and NuA4 can be direct, we performed a GST pulldown experiment using recombinant GST-Sfp1 and TAP-purified NuA4. NuA4 activity was assessed by a HAT assay on

nucleosomes. GST-Gcn4 is used as a positive control as Gcn4-NuA4 interaction is known [30]. As shown in Fig 1D, NuA4 HAT activity is pulled down by GST-Sfp1 and GST-Gcn4 but not GST alone, with parallel depletion from the supernatant. Altogether, these results indicate that Sfp1 interacts with NuA4 *in vivo* and this interaction is likely direct.

Sfp1 does not affect NuA4 binding at RP and RiBi gene promoters

Since Sfp1 and NuA4 physically interact, we next determined if Sfp1 affects NuA4 recruitment at the promoters of RiBi and RP genes. Cells lacking Sfp1 exhibit reduced size and slower growth rate compared to wild-type cells [6, 31, 32]. To avoid the negative impact of Sfp1 deletion on growth that could lead to indirect effects, we used the "anchor-away" (AA) system to rapidly deplete Sfp1 from the nucleus [33]. AA-induced Sfp1 depletion results in noticeable growth defects on plates while robust growth is maintained in control conditions (Fig 2A). Sfp1 depletion from its target genes was confirmed by chromatin immunoprecipitation (ChIP) at *RPL2B* and *RPS11B* promoters (Fig 2B-C). Interestingly, the binding of NuA4 (Eaf1 subunit) does not seem affected by Sfp1 presence (Fig 2D). Even the use of *SFP1*-deleted cells confirmed that NuA4 binding at RP promoters is not significantly affected by the absence of Sfp1 (S1A-B Fig). Furthermore, even overexpression of *SFP1* from the inducible *GAL1* promoter does not affect NuA4 binding (S1C-D Fig).

We next sought to examine Sfp1 and NuA4 localization genome-wide. Discrepancies in previous studies on Sfp1 localization stemmed from limited detection at only a subset of RP gene promoters, while both RP and RiBi genes are downregulated in *sfp1Δ* strains [6, 31]. Also, gene expression analysis from a Gal-induced Sfp1 expression revealed rapid induction of RiBi

genes, whereas RP gene expression is increased with much slower kinetics [32]. In contrast to ChIP experiments which predominantly detected Sfp1 binding at RP gene promoters, ChEC-seq using MNase-based chromatin digestion showed clear Sfp1 signals at RiBi genes with limited detection at RP gene promoters [25, 34, 35]. This methodological discrepancy may be attributed to the higher A/T content and lower formaldehyde-crosslinking efficiency of RiBi gene promoters compared to RP genes [5, 36-39]. To address this issue, we used the non-crosslinking CUT&RUN approach to analyze NuA4 and Sfp1 profiles [40, 41]. This technique is related to the ChEC-seq method while addressing its limitations due to the target proteins being fused with the MNase enzyme. For analysis, we categorized the detectable genes into three clusters: RP genes, RiBi genes, and RiBi-like genes (other Sfp1-targeted genes that exhibit similar regulation to RiBi genes) [25].

CUT&RUN signals for NuA4 confirm binding at both RP and RiBi gene promoters, with stronger signals observed for RP genes (Fig 3A). Consistent with our ChIP-qPCR data, Sfp1 depletion does not negatively affect NuA4 binding across all three gene clusters (Fig 3B). Thus, we conclude that the recruitment of the NuA4 complex is independent of its association with Sfp1.

Sfp1 depletion attenuates acetylation of histone H3, H4 and Htz1

While the recruitment of NuA4 is not affected by Sfp1, we tested whether Sfp1 influences its function. Nucleosomes surrounding the Upstream Activating Sequences (UAS) of RP/RiBi genes are highly acetylated reflecting chromatin structure permissive for transcription[13]. Histone H3 and H4 acetylation levels were measured by ChIP-seq, using total histone H3 signal as control

for nucleosome occupancy, in biological duplicates. Box plots shown in Fig 4A indicate that depletion of Sfp1 induces a statistically significant reduction in both H3 and H4 acetylation at all gene clusters (also see heatmaps in S2 Fig). These results suggest that the presence of Sfp1 at RP/RiBi genes may set the promoter architecture to facilitate histone H4 acetylation without affecting the binding of NuA4.

Htz1 is a histone H2A variant often found at promoter regions [42]. It has a unique C-terminal tail that plays a crucial role in its deposition, and an extended αC helix patch that regulates chromatin compaction [43, 44]. Gene activation promotes Htz1 loss, whereas gene repression promotes Htz1 acquisition [42]. Interestingly, Htz1 is highly enriched in RiBi genes whereas RP genes are depleted of Htz1 [42]. Surprisingly, ChIP-seq data both show a significant increase in Htz1 occupancy at RiBi and RiBi-like gene promoters upon Sfp1 depletion (Fig 4A, Htz1/H3). NuA4 can regulate Htz1 incorporation and is responsible for its acetylation in chromatin [21, 45-47]. To measure Htz1 acetylation, we immunoprecipitated proteins using an anti-acetylated lysine (anti-Kac) antibody and measured Htz1 changes by western blotting. When Sfp1 is depleted, we observe a slight decrease in Htz1 acetylation while bulk H4 acetylation remains unchanged (Fig 4B). Anti-Htz1K14ac antibody was also used to measure NuA4-dependent acetylation by ChIP-qPCR and shows a decrease at RiBi gene promoters in the absence of Sfp1 (Fig 4C-4E). *SFP1*-deleted cells also show a decrease in bulk Htz1K14 acetylation, as well as an apparent increase in total Htz1 (S3A Fig). Comparison of Sfp1 CUT&RUN peaks with published Htz1 ChIP-seq peaks [48] indicates that the majority of Sfp1 bound regions also contain Htz1 (S3B Fig). These findings are consistent with previous studies linking Htz1K14 acetylation to active genes, including Sfp1 target genes involved in ribosome biogenesis and

protein synthesis [47]. Our results show that Sfp1 affects NuA4-dependent acetylation of histone H4 and Htz1 as well as SAGA-mediated acetylation of histone H3. Furthermore, decrease of acetylation in the absence of Sfp1 leads to stabilization of Htz1 at RiBi promoters. These observations suggest that Sfp1 indirectly modulates chromatin structure by affecting histone acetylation and the stability of Htz1-containing nucleosomes.

NuA4 depletion leads to decreased Sfp1 binding at ribosomal protein gene promoters

Since Sfp1 does not affect the binding of NuA4 at promoters but can modulate its function, we tested if NuA4 can affect Sfp1 function at co-bound promoters. Since Esa1 is essential for viability, we relied again on the anchor-away approach to rapidly deplete NuA4 catalytic subunit Esa1 (Fig 5A). One hour of Esa1 depletion leads to reduction of H4 acetylation in bulk chromatin as well as by ChIP-qPCR at RP/RiBi genes (Fig 5B-C). We then assessed by CUT&RUN the effect of NuA4 depletion on Sfp1 presence at target genes. Upon Esa1 depletion, Sfp1 binding is reduced at the RP gene cluster (Fig 5D). In yeast, ribosomes are composed of 79 distinct RPs encoded by 138 genes. Several TFs, including Rap1, Hmo1, Ifh1, Fhl1, and Sfp1, have been found to localize at the promoter of RP genes. Distinct binding patterns of these TFs are used to categorize RP genes into three groups [3, 5, 49, 50]. Hmo1 specifically binds to Cat I promoters, while both Cat I and II promoters show detectable binding of Rap1, Ifh1, Fhl1, and Sfp1. Cat III promoters have different architectures, with only 13 RP genes in this category [39]. Notably, Sfp1 has been shown to bind the gAAAATTTTc motif *in vitro* and may be present on the Cat III promoters [3, 51]. When Sfp1 is rapidly depleted, there is a much stronger down-regulation of Cat III genes compared to Cat I and II [25]. Therefore, to more precisely assess the

role of NuA4 on Sfp1 binding at RP gene promoters, we divided the RP cluster into these three categories and analyzed our Sfp1 CUTnRUN data. Box plots in Fig 5E show that Sfp1 is detectable in all three categories, although Cat III promoters had the lowest signal. Importantly, a significant decrease in Sfp1 signal is observed upon Esa1 depletion in the Cat I and II groups, whereas Sfp1 binding at Cat III genes is not affected. Representative IGV tracks for all three categories are shown in Fig 5F. These results clearly indicate that NuA4 is required for optimal recruitment of Sfp1 to Cat I and II RP genes.

Sfp1 is acetylated by NuA4 at lysines 655 and 657

In addition to histones, NuA4 can acetylate non-histone substrates that are involved in a variety of cellular processes [52-55]. Previous observations indicate that Sfp1 is acetylated on lysines 655 and 657 *in vivo* and this modification is Esa1/NuA4-dependent [56] (Fig 6A). To test the relative contribution of these two acetylation sites to Sfp1 function, we generated a K655/657 arginine mutant (K655/657R), which cannot be acetylated but maintains the positive charge of lysine residues, and a K655/657 glutamine mutant, which is often used as a mimic of acetylated lysine residues (K655/657Q). The R and Q mutants have the same protein level as the wild-type Sfp1 but we observed a slightly slower growth for the Q mutant in liquid media (S4A-S4B Fig). We first wanted to confirm that Sfp1 is acetylated *in vivo* and assess the contribution of the two lysine residues. We immunoprecipitated Sfp1 from wild-type and mutated strains and performed Western blotting using an anti-acetyllysine antibody. We also assessed Sfp1 acetylation level in a *sir2Δhst1Δhst2Δ* deacetylase mutant strain (ΔHDACs) and confirmed previous results as acetylated Sfp1 is significantly increased in that genetic background [56]. As

shown in Fig 6B, Sfp1 is acetylated *in vivo* and the K655/657R mutation slightly reduces the level of acetylated Sfp1 without eliminating it. This suggests that K655/657 are indeed targeted for acetylation but are not the only sites on Sfp1. It also indicates that these sites show dynamic acetylation/deacetylation cycles involving sirtuins deacetylases (Fig 6B).

In optimal growth conditions, Sfp1 is localized in the nucleus and moves out to the cytoplasm when yeast cells undergo stress or nutritional deprivation [10]. As mentioned above, the TORC1 Complex promotes Sfp1 nuclear localization [6] and its inhibition by rapamycin strongly affects Sfp1 localization and function. Interestingly, the Sfp1 K655/K657Q acetyl-mimic mutant cells have increased sensitivity to rapamycin compared to wild-type and K655/657R mutant cells (Fig 6C). In parallel, the ΔHDACs strain is highly sensitive to TOR1 inhibition but the K655/657R mutant cannot rescue this phenotype by itself (Fig 6D). These results suggest that mutations in Sfp1 mimicking constitutive acetylation makes the cells more sensitive to inhibition of TOR signaling, perhaps acting like a misleading signal of high nutrient conditions. To dissect the effects of NuA4-dependent Sfp1 acetylation on Sfp1 binding to target genes, we performed Sfp1 CUT&RUN sequencing under normal and TOR1-inhibited conditions. Intriguingly, the binding of the acetyl-mimic Sfp1 is significantly increased at RiBi and RiBi-like genes when growth conditions are favourable, while no significant change is observed at RP gene promoters (Fig 6E and 6F). In contrast, the opposite trend occurs upon rapamycin treatment, as the acetyl-mimic Sfp1 shows significant decreased binding at all gene clusters (Fig 6F). This is consistent with the slower growth rate in the presence of rapamycin, the acetyl-mimic mutant being more sensitive to TORC1 inhibition than wild-type Sfp1. Importantly, NuA4 recruitment is also increased at RiBi and RiBi-like gene promoters in rich media in the presence of Sfp1-K655/657Q

as well as also decreased after rapamycin treatment in the same background, functionally linking again Sfp1 acetylation and NuA4 (Fig 6G). Altogether, these results suggest that constitutive acetylation of Sfp1 is an aberrant signal misleading the cell in different growth conditions.

Acetylation of Sfp1 affects its activity as transcriptional activator

Since the binding of Sfp1 to target genes can be affected by its NuA4-dependent acetylation, we analyzed its effect on transcription. RNAs were extracted from wild-type Sfp1 and the two mutant strains grown in rich media and differentially expressed genes were measured by RT-qPCR. The K655/657Q strain shows more than two-fold increase in the expression of RiBi genes, while RP gene expression remains similar to that of the wild-type strain (Fig 7A). To get the genome-wide picture, we then performed RNA sequencing. As shown in Fig 7B-7D, genes belonging to RiBi and RiBi-like clusters are confirmed as upregulated in the Sfp1 acetyl-mimic mutant. Altogether, these results demonstrate that NuA4-dependent acetylation of Sfp1 has a significant impact on its binding and function regulating specific classes of genes. This is also reminiscent of previous observations showing that overexpression of Sfp1 upregulates a large number of genes involved in ribosome biogenesis, leading to a slow-growth phenotype [8]. Similarly, the same set of genes related to metabolic pathways is down-regulated in K655/657Q mutant and Sfp1-overexpressing cells (S5 Fig) [25].

Carbon source shift and glucose pulse experiments reveal different Sfp1 regulatory mechanisms toward RiBi and RP gene clusters

Yeast cells deleted for *SFP1* are characterized by carbon source-dependent slow growth and small sizes [31, 32]. While glucose is the preferred carbon source, yeast can also ferment raffinose as a non-permissive carbon source, but at a lower growth rate. We repeated RNA extraction, RT-qPCR and RNA-seq with the wild-type and mutant strains but this time in raffinose-containing media (Fig 8). When growing in the media where raffinose is the sole carbon source, RP genes are downregulated in all tested strains. However, RiBi genes seem to some extent upregulated (Fig 8A). Strikingly, with this carbon source, an opposite effect is seen with the Sfp1 acetyl-mimic mutant, with RiBi and RiBi-like genes being down-regulated (Fig 8A-D). These results are certainly consistent with the Sfp1 CUT&RUN data showing that binding of the acetyl-mimic Sfp1 is more sensitive to stress/nutrient starvation (Fig 6F).

To better understand the different effects of carbon sources and eliminate growth rate influences, we conducted a carbon source shift assay, adding glucose back after incubation in raffinose. This assay allowed us to study how cells detect changes in nutrient availability and adjust their metabolism. Fig 9A illustrates the procedure of the assay. Both K655/657 mutants (R and Q) and reference strains were grown in rich YPD media (2% glucose) until the early exponential phase. Cells were then washed to remove glucose and incubated in YPR (2% raffinose) for one generation. Glucose was then reintroduced to the media and gene expression was monitored at different time points.

As expected, RT-qPCR data show that the expression of both RP and RiBi genes increases immediately upon the addition of glucose (Fig 9B-9E, S6A Fig). The Sfp1 K655/657R mutant and wild-type strains show similar expression levels of all tested RP genes during the glucose pulse period, while RiBi genes seem slightly more expressed in the K655/657R mutant. However,

global analysis by RNA-seq reveals that the K655/657R mutant, while confirming more expression of RiBi genes, also shows significant more expression of RP genes compared to wild-type cells (Fig 9F-9G). These results indicate that, although the K655/657R mutant does not show growth phenotype under normal conditions, Sfp1 function is still affected under poor conditions when cells are suddenly pushed to their potential by rapid transcriptional reprogramming upon addition of optimal carbon source. In parallel, despite the RiBi gene expression differences compared to wild-type cells, the acetyl-mimic Sfp1 mutant is able to drive RiBi gene transcription to a level similar to wild-type cells upon the glucose pulse (Fig 9G). Interestingly, RP gene upregulation with the addition of glucose shows a clearly different regulatory mechanism since the K655/657Q mutant does not show capacity to express RP genes to the same level as the wild-type cells during the glucose pulse (Fig 9F, S6B Fig).

Discussion

In the present work, we demonstrate that the Sfp1 transcription activator interacts with the coactivator NuA4 complex to coregulate ribosomal protein and ribosome biogenesis gene expression. The presence of Sfp1 at the RiBi and RP gene promoters is important for the NuA4-mediated local histone H4 acetylation. Despite NuA4 binding to promoters not being affected by Sfp1, its function as acetyltransferase seems attenuated with Sfp1 depletion. We also revealed that histone variant Htz1 occupancy increases whereas its acetylation levels decrease upon Sfp1 depletion. NuA4-dependent Htz1 acetylation near gene promoters was reported to be linked to transcription activation since it favors nucleosome disassembly [42, 47]. These results indicate that Sfp1 may facilitate gene transcription via NuA4-dependent Htz1 acetylation. Our previous

work showed that NuA4-mediated H4 acetylation can increase Htz1 incorporation which could also be at play in NuA4 and Sfp1 functional interaction [46]. In addition, NuA4 has a clear positive impact on Sfp1 binding at RP genes in optimal growth conditions, indicating bi-directional functional cooperation (Fig 10A).

The physical interaction described here between NuA4 and Sfp1 is also reminiscent of the protein JAZF1, the homolog of Sfp1 in mammals. JAZF1 is strongly linked to cellular metabolism, being implicated in glucose and lipid homeostasis, insulin signaling, and metabolic disorders such as diabetes [57]. Strikingly, JAZF1 has recently been identified as a stoichiometric subunit of the human NuA4/TIP60 complex [58]. Furthermore, the depletion of JAZF1 can lead to reduced H2A.Z acetylation at NuA4/TIP60 regulatory sites [59]. Thus, the physical and functional interaction between NuA4 and Sfp1 seems conserved throughout eukaryotes and play a major role in regulating cell homeostasis.

The fact that Sfp1 is directly acetylated by NuA4 is certainly part of signaling events regulating its function upon changes in growth conditions. Cells expressing acetyl-mimic mutant Sfp1 exhibit abnormal transcription profile that includes augmented RiBi gene expression under normal growth conditions and reduced RiBi gene expression under stress/poor carbon source, both linked to level of Sfp1 binding to the promoters (Fig 10B). The high availability of acetyl-CoA in rich media may be part of the process leading to Sfp1 acetylation by NuA4, signaling optimal conditions for growth, hence ribosome biogenesis/translation. But this possible link with acetyl-CoA does not fit with how the acetyl-mimic mutant misleads the cells in poor conditions, in this case seemingly overcompensating by showing reduced expression of RiBi genes. One model to reconcile those results could argue that cycles of Sfp1 acetylation and

deactylation serve as a rheostat to ensure proper transactivator activity, not too high or too low. Due to the complexity of RP gene regulation under steady state conditions, only an impact of the Q mutant on RiBi genes can be seen, but contributions of both K-R and K-Q mutants are seen during nutrient shifts. Importantly, in these shifting conditions, the mutants show opposite effects on RP genes, as one might predict (Fig 9F).

The glucose pulse experiment allowed us to explore different transcriptional mechanisms between RiBi genes and RP genes mediated by Sfp1, before other mechanisms of regulation kick in at steady state levels. As mentioned before, RiBi gene promoters have two distinct motifs indicating that RiBi gene regulations are partially different from RP genes. Also, transcription factor Ifh1, which binds RP gene promoters, affects Sfp1 binding only at RP genes [25] and is itself regulated by acetylation, although through Gcn5/SAGA instead of Esa1/NuA4 [12]. Interestingly, Ifh1 acetylation titrates its activator function after being bound the RP promoters and it is tempting to speculate a related fine-tuning function of Sfp1 acetylation by NuA4 at RiBi genes. Constitutive Sfp1 acetylation may lead to aberrant cell response to nutrient perturbations through specific regulatory mechanisms towards different targeted gene clusters. A deeper mechanistic understanding will require precise measurement of Sfp1 acetylation in different conditions as well as characterizing other lysine residues being targeted.

Acknowledgments

We are grateful to Steven Henikoff for providing Protein A-MNase used in CUT&RUN experiments. This work was supported by grants from the Canadian Institutes of Health Research (CIHR) to J.C. (FDN-143314, PJT-183708). K.X. was supported by a scholarship from the

Chinese Academy of Science. J.C. held a Canada Research Chair (Tier 1) in Chromatin Biology and Molecular Epigenetics.

Methods

Yeast strains and spot assay

Yeast strains used in this study are listed in S1 Table and were constructed based on standard PCR-based transformation protocol. All strains generated were verified using PCR and sequencing. Unless indicated, Yeast cells were grown in YPD (1% yeast extract, 2% peptone, 2% dextrose) at 30°C. The anchor-away parental strain used for transformation was previously mutated (*tor1-1* mutation and *FPR1* deletion) to make the cells resistant to rapamycin, while Rpl13a was tagged with FKBP12, as described [33]. For Esa1 N-terminal tagging, the FRB tag was inserted after the start codon as described [60]. Cells were treated with rapamycin at 1 µg/mL for anchor-away-induced depletion. For spot assays, single colonies from fresh plates were grown overnight in YPD at 30°C. Cell cultures were diluted in fresh YPD to OD_{600} 0.3 and continued to grow until OD_{600} 0.7-0.8. The 10-fold serial dilutions of the yeast cultures were made for each strain and 4 µL of each dilution was spotted on plates. Colonies were incubated at 30°C for 2-4 days, then the growth sensitivities were compared between plates.

GST purification and HAT assay

Recombinant Sfp1 was purified from BL-21 bacteria transformed with pGEX-4T-3-GST-*SFP1* and induced with 500 nM IPTG overnight at 16°C. Bacterial pellets were lysed with lysozyme and sonicated. After clarification by centrifugation, soluble fractions were incubated with Glutathione-Sepharose beads (GE Healthcare) for 3 hours at 4°C. Beads were washed and ready

to use. GST-immobilized Sfp1 proteins were incubated with TAP-purified NuA4 complex for 4 hours at 4°C. After incubation, the supernatant was collected, and the beads were washed. Histone acetyltransferase (HAT) assay was performed as described [61, 62]. 500ng of short oligonucleosomes purified from MNase-digested yeast chromatin was incubated with the GST beads or the supernatant mentioned before at 30°C for 30 minutes. 0.125 µCi of [3H] acetyl coenzyme A ([3H] acetyl-CoA) was added in HAT buffer (50 mM Tris-HCl [pH 8], 50 mM KCl plus NaCl, 0.1 mM EDTA, 5% glycerol, 1 mM DTT, 1 mM PMSF and 20 mM sodium butyrate). The reactions were stopped in 1X Laemmli buffer, boiled and loaded on a 10% SDS-PAGE. Gel was treated with En3hance (Perkin Elmer), dried and exposed on film.

Chromatin immunoprecipitation (ChIP)

200 mL cell cultures were collected at OD_{600} 0.7-0.8. Cells were crosslinked with 1% formaldehyde for 20min and quenched by adding 125 mM glycine for 5min. Sonication was performed to obtain 200-500bp chromatin fragments. 100 ug of chromatin was incubated with indicated antibodies for each IP. Magnetic beads were added, and the mix was incubated for 3-4 hours at 4°C. The chromatin was eluted from beads after wash. The eluate was incubated overnight at 65 °C to reverse the crosslinks. Phenol chloroform extraction was performed and 1uL of each DNA sample was used for qPCR. ChIP-qPCR data are presented as % of IP/Input (or ratio of IP/Input when correcting for nucleosome occupancy, i.e. H4K8ac/H3) and are from at least two independent yeast cultures in each experiment. Lists of primers standardized on a LightCycler qPCR apparatus are available upon request. For ChIP-sequencing, libraries were prepared as described [63]. Samples were sequenced 100-bp paired-end for around 10M reads per sample. Sequencing was performed at IRCM (Montreal Clinical Research Institute).

Antibodies used were against H4K8ac (Abcam, ab45166), H3K9ac (Upstate, #07-352), Htz1.K14ac (Upstate, #07-719), H3 (Abcam, ab1791), Htz1 (Millipore, #07-718), Eaf1(homemade), Myc (Sigma, M5546).

Acetyl-lysine Immunoprecipitation

Immunoprecipitation was performed as described previously [64]. Cells were grown in YPD till OD600 around 0.5 followed by rapamycin (1 µg/mL final) or vehicle treatment for 2 hours. Cells were collected and lysed in lysis buffer (10 mM Tris-HCL pH 8.0, 150 mM NaCl, 10% glycerol, 0.1% NP-40, 2 µg/mL leupeptin, 2 µg/mL pepstatin A, 5 µg/mL aprotinin, 1 mM PMSF, 10 mM *β*-glycerophosphate, 1mM Sodium Butyrate, 0.5 mM NaF, and 1 mM DTT). 6 µg of WCE was incubated with anti-acetyl (ImmuneChem ICP0380) overnight at 4°C. Protein G magnetic beads (Invitrogen 1004D) were added and incubated for 4 additional hours. Beads were washed and 1X Laemmli buffer was added. The samples were then loaded on SDS-PAGE.

RT-qPCR and RNA-sequencing

Total RNA was extracted following the hot-phenol protocol. In brief, cell pellets were resuspended in 400 µL TES solution (10 mM Tris HCl, 10 mM EDTA, and 0.5% SDS). 400 µL acid phenol was added and then vortexed. The cell suspensions were incubated at 65 ˚ C for 30 minutes with occasional, brief vortexing. Top speed centrifuge was performed to separate the aqueous phase. The aqueous phase was transferred and 400 µL chloroform was added followed by another round of vortex and centrifuge. RNAs were precipitated with sodium acetate and 100% ethanol. Initial precipitated RNAs were washed with ice-cold 70% ethanol. RNA pellets were resuspended in 50 µL RNase-free H_2O. Reverse transcription was performed following the 2X SYBR Green PCR Master Mix kits protocol. qPCR was performed using indicated primers to

test specific gene expression and normalized to ACT1 expression level. For RNA-Seq, the NEBNext ultra II RNA library prep kit was used for library preparation. The sequencing run was performed on an Illumina NovaSeq 6000 system. Reads were trimmed using fastp v0.23.2 [65]. Quality check was performed on raw and trimmed data to ensure the quality of the reads using FastQC v0.11.9 and MultiQC v1.12 [66]. The quantification was performed with Kallisto v0.48.0 [67] against the Saccharomyces cerevisiae transcriptome (R64-1-1 downloaded from Ensembl release 109). The principal component analysis was completed with the FactoMineR v2.7 R package [68] and the graphical representations were produced with the ggplot2 v3.4.2 package [69]. Differential expression analysis was performed using the DESeq2 v1.38.3 package [70]. Genes were considered significantly dysregulated for absolute fold change ratio >=1.5 and adjusted p-value <0.05. The volcano graphical representations were produced with the EnhancedVolcano v1.18.0 package. GO enrichment analysis was carried out using clusterProfiler v4.8.3 with an adjusted p-value cutoff of 0.05 and the function “simplify” to reduce the redundancy of GO terms enriched with the default parameters [71]. Box plots and associated Wilcoxon tests were generated using the ggboxplot and stat_compare_means functions, respectively, with the default settings of the ggpubr v0.5.0 package (https://CRAN.R-project.org/package=ggpubr). Heat maps were generated using ComplexHeatmap v2.10.0 package [72]. All R analysis were done in R v4.2.2.

CUT&RUN Sequencing

The experiment was performed as described [41]. Yeast nuclei were freshly prepared according to published procedures [73] and bound to concanavalin A beads. The beads were then resuspended in a buffer containing digitonin, and antibodies (Eaf1, Myc and IgG) were added to

incubate overnight at 4°C. Afterward, the beads were washed, and pA-MNase (provided by Steven Henikoff) was added. One-hour secondary antibody incubation was performed for samples using anti-Myc antibody. CaCl2 was added to activate MNase digestion for 5 to 15 minutes. The reaction was quenched by the addition of stop buffer containing EDTA and EGTA. DNA was purified with NEB Monarch PCR and DNA purification kit following the protocol. DNA was quantified by Qubit HS DNA kit. The library was prepared following the manufacturer's instructions in NEBNext Ultra II DNA kit for low-input ChIP. 100-bp pair-end sequencing was performed with the Illumina NovaSeq 6000 system. Raw reads were trimmed using fastp v0.20.1 [65]. Trimmed reads were aligned on the Saccharomyces cerevisiae genome (R64-1-1 - sacCer3) using bwa mem v0.7.17 [74] and samtools v1.13 [75]. The macs2 v2.2.1 software [76] was used to perform the peak calling and regions were annotated using the ChIPseeker package v1.30.3 [71] in R v4.1.2. Raw signal tracks and normalized tracks (in reads per million, RPM) were produced from mapped reads using deepTool's bamCoverage tool v3.3.0 [77] and bedtools genomecov tool v2.17.0 [78], respectively. Tracks were converted to the bigwig format using bedGraphToBigWig v2.8 [79] and signal tracks were visualized with IGV [80]. For transcription factors, IgG negative control tracks were subtracted from normalized RPM tracks using deepTools 'bigwigCompare' [77]. For histone marks, signal tracks were normalized to histone H3 levels. Cut&Run reads mapping were then divided into promoter groups of genes (RIBI, RIBI-like, RP genes and subcategories) for the generation of heat maps using ComplexHeatmap v2.10.0 [72] and EnrichedHeatmap v1.24.0 [81] packages. Box plots and associated Wilcoxon tests were computed using means of bins per gene and were produced using the ggboxplot and stat_compare_means functions, respectively, with the default settings

of the ggpubr v0.5.0 package (https://CRAN.R-project.org/package=ggpubr). Publicly available Htz1 ChIP-seq data in wild-type yeast were obtained from Gene Expression Omnibus (GEO) under accession code GSE54105. Following alignment and peak calling as previously described, the intersection of Htz1 genomic regions with Sfp1 peaks was completed using Intervene v0.6.5 [82].

Carbon shift and glucose pulse assay

Yeast cells were grown in YPD overnight at 30 ˚C to the exponential phase. The next day, cells were collected by centrifugation and washed twice with water before resuspending in the media containing 2% raffinose as the single carbon source. Glucose was then added to the culture to a final 2% after raffinose incubation. Total RNA was extracted at 15min, 30min and 60min upon glucose addition.

Data availability

NGS assays reported in this study are available at the GEO repository under the following accession numbers: ChIP-seq data (GSE267779, Token: kpylmiiibnubbep), RNA-seq data (GSE268202,Token: kxqzaaygzbyrjez), CUT&RUN-seq data (GSE267939, Token: cjizweiyrhgfbgb).

References

1. Gasch AP, Spellman PT, Kao CM, Carmel-Harel O, Eisen MB, Storz G, et al. Genomic expression programs in the response of yeast cells to environmental changes. Mol Biol Cell. 2000;11(12):4241-57. doi: 10.1091/mbc.11.12.4241. PubMed PMID: 11102521; PubMed Central PMCID: PMCPMC15070.
2. González A, Hall MN. Nutrient sensing and TOR signaling in yeast and mammals. Embo j. 2017;36(4):397-408. Epub 20170117. doi: 10.15252/embj.201696010. PubMed PMID: 28096180; PubMed Central PMCID: PMCPMC5694944.
3. Zencir S, Dilg D, Rueda MP, Shore D, Albert B. Mechanisms coordinating ribosomal protein gene transcription in response to stress. Nucleic Acids Res. 2020;48(20):11408-20. doi: 10.1093/nar/gkaa852. PubMed PMID: 33084907; PubMed Central PMCID: PMCPMC7672434.

4. Raué HA, Planta RJ. Ribosome biogenesis in yeast. Prog Nucleic Acid Res Mol Biol. 1991;41:89-129. doi: 10.1016/s0079-6603(08)60007-0. PubMed PMID: 1882079.
5. Shore D, Zencir S, Albert B. Transcriptional control of ribosome biogenesis in yeast: links to growth and stress signals. Biochem Soc Trans. 2021;49(4):1589-99. doi: 10.1042/BST20201136. PubMed PMID: 34240738; PubMed Central PMCID: PMCPMC8421047.
6. Jorgensen P, Rupes I, Sharom JR, Schneper L, Broach JR, Tyers M. A dynamic transcriptional network communicates growth potential to ribosome synthesis and critical cell size. Genes Dev. 2004;18(20):2491-505. Epub 20041001. doi: 10.1101/gad.1228804. PubMed PMID: 15466158; PubMed Central PMCID: PMCPMC529537.
7. Bosio MC, Negri R, Dieci G. Promoter architectures in the yeast ribosomal expression program. Transcription. 2011;2(2):71-7. doi: 10.4161/trns.2.2.14486. PubMed PMID: 21468232; PubMed Central PMCID: PMCPMC3062397.
8. Fingerman I, Nagaraj V, Norris D, Vershon AK. Sfp1 plays a key role in yeast ribosome biogenesis. Eukaryot Cell. 2003;2(5):1061-8. doi: 10.1128/EC.2.5.1061-1068.2003. PubMed PMID: 14555489; PubMed Central PMCID: PMCPMC219361.
9. Lempiainen H, Uotila A, Urban J, Dohnal I, Ammerer G, Loewith R, et al. Sfp1 interaction with TORC1 and Mrs6 reveals feedback regulation on TOR signaling. Mol Cell. 2009;33(6):704-16. doi: 10.1016/j.molcel.2009.01.034. PubMed PMID: 19328065.
10. Marion RM, Regev A, Segal E, Barash Y, Koller D, Friedman N, et al. Sfp1 is a stress- and nutrient-sensitive regulator of ribosomal protein gene expression. Proc Natl Acad Sci U S A. 2004;101(40):14315-22. Epub 20040907. doi: 10.1073/pnas.0405353101. PubMed PMID: 15353587; PubMed Central PMCID: PMCPMC521938.
11. Robert F, Pokholok DK, Hannett NM, Rinaldi NJ, Chandy M, Rolfe A, et al. Global position and recruitment of HATs and HDACs in the yeast genome. Mol Cell. 2004;16(2):199-209. doi: 10.1016/j.molcel.2004.09.021. PubMed PMID: 15494307; PubMed Central PMCID: PMCPMC3004369.
12. Downey M, Knight B, Vashisht AA, Seller CA, Wohlschlegel JA, Shore D, et al. Gcn5 and sirtuins regulate acetylation of the ribosomal protein transcription factor Ifh1. Curr Biol. 2013;23(17):1638-48. Epub 20130822. doi: 10.1016/j.cub.2013.06.050. PubMed PMID: 23973296; PubMed Central PMCID: PMCPMC3982851.
13. Rossetto D, Cramet M, Wang AY, Steunou AL, Lacoste N, Schulze JM, et al. Eaf5/7/3 form a functionally independent NuA4 submodule linked to RNA polymerase II-coupled nucleosome recycling. EMBO J. 2014;33(12):1397-415. Epub 20140519. doi: 10.15252/embj.201386433. PubMed PMID: 24843044; PubMed Central PMCID: PMCPMC4194127.
14. Cai L, Sutter BM, Li B, Tu BP. Acetyl-CoA induces cell growth and proliferation by promoting the acetylation of histones at growth genes. Mol Cell. 2011;42(4):426-37. doi: 10.1016/j.molcel.2011.05.004. PubMed PMID: 21596309; PubMed Central PMCID: PMCPMC3109073.
15. Uprety B, Sen R, Bhaumik SR. Eaf1p Is Required for Recruitment of NuA4 in Targeting TFIID to the Promoters of the Ribosomal Protein Genes for Transcriptional Initiation In Vivo. Mol Cell Biol. 2015;35(17):2947-64. Epub 20150622. doi: 10.1128/MCB.01524-14. PubMed PMID: 26100014; PubMed Central PMCID: PMCPMC4525319.

16. Brown CE, Howe L, Sousa K, Alley SC, Carrozza MJ, Tan S, et al. Recruitment of HAT complexes by direct activator interactions with the ATM-related Tra1 subunit. Science. 2001;292(5525):2333-7. doi: 10.1126/science.1060214. PubMed PMID: 11423663.
17. Steunou A-L, Rossetto D, Côté J. Regulating Chromatin by Histone Acetylation. In: Workman JL, Abmayr SM, editors. Fundamentals of Chromatin. New York, NY: Springer New York; 2014. p. 147-212.
18. Doyon Y, Cote J. The highly conserved and multifunctional NuA4 HAT complex. Curr Opin Genet Dev. 2004;14(2):147-54. doi: 10.1016/j.gde.2004.02.009. PubMed PMID: 15196461.
19. Babiarz JE, Halley JE, Rine J. Telomeric heterochromatin boundaries require NuA4-dependent acetylation of histone variant H2A.Z in Saccharomyces cerevisiae. Genes Dev. 2006;20(6):700-10. doi: 10.1101/gad.1386306. PubMed PMID: 16543222; PubMed Central PMCID: PMCPMC1413290.
20. Boudreault AA, Cronier D, Selleck W, Lacoste N, Utley RT, Allard S, et al. Yeast enhancer of polycomb defines global Esa1-dependent acetylation of chromatin. Genes Dev. 2003;17(11):1415-28. doi: 10.1101/gad.1056603. PubMed PMID: 12782659; PubMed Central PMCID: PMCPMC196073.
21. Keogh MC, Mennella TA, Sawa C, Berthelet S, Krogan NJ, Wolek A, et al. The Saccharomyces cerevisiae histone H2A variant Htz1 is acetylated by NuA4. Genes Dev. 2006;20(6):660-5. doi: 10.1101/gad.1388106. PubMed PMID: 16543219; PubMed Central PMCID: PMCPMC1413285.
22. Reid JL, Iyer VR, Brown PO, Struhl K. Coordinate regulation of yeast ribosomal protein genes is associated with targeted recruitment of Esa1 histone acetylase. Mol Cell. 2000;6(6):1297-307. doi: 10.1016/s1097-2765(00)00128-3. PubMed PMID: 11163204.
23. Rohde JR, Cardenas ME. The tor pathway regulates gene expression by linking nutrient sensing to histone acetylation. Mol Cell Biol. 2003;23(2):629-35. doi: 10.1128/mcb.23.2.629-635.2003. PubMed PMID: 12509460; PubMed Central PMCID: PMCPMC151550.
24. Joo YJ, Kim JH, Kang UB, Yu MH, Kim J. Gcn4p-mediated transcriptional repression of ribosomal protein genes under amino-acid starvation. Embo j. 2011;30(5):859-72. Epub 20101224. doi: 10.1038/emboj.2010.332. PubMed PMID: 21183953; PubMed Central PMCID: PMCPMC3049204.
25. Albert B, Tomassetti S, Gloor Y, Dilg D, Mattarocci S, Kubik S, et al. Sfp1 regulates transcriptional networks driving cell growth and division through multiple promoter-binding modes. Genes Dev. 2019;33(5-6):288-93. Epub 20190225. doi: 10.1101/gad.322040.118. PubMed PMID: 30804227; PubMed Central PMCID: PMCPMC6411004.
26. Jiang Y, Berg MD, Genereaux J, Ahmed K, Duennwald ML, Brandl CJ, et al. Sfp1 links TORC1 and cell growth regulation to the yeast SAGA-complex component Tra1 in response to polyQ proteotoxicity. Traffic. 2019;20(4):267-83. doi: 10.1111/tra.12637. PubMed PMID: 30740854.
27. Zheng Q, Qiu H, Zhang H, Hinnebusch AG. Differential requirements for Gcn5 and NuA4 HAT activities in the starvation-induced versus basal transcriptomes. Nucleic Acids Res. 2023;51(8):3696-721. doi: 10.1093/nar/gkad099. PubMed PMID: 36864781; PubMed Central PMCID: PMCPMC10164569.

28. Joo YJ, Buratowski S. Gds1 Interacts with NuA4 To Promote H4 Acetylation at Ribosomal Protein Genes. Mol Cell Biol. 2022;42(1):e0037321. Epub 20211025. doi: 10.1128/mcb.00373-21. PubMed PMID: 34694912; PubMed Central PMCID: PMCPMC8773082.
29. Auger A, Galarneau L, Altaf M, Nourani A, Doyon Y, Utley RT, et al. Eaf1 is the platform for NuA4 molecular assembly that evolutionarily links chromatin acetylation to ATP-dependent exchange of histone H2A variants. Mol Cell Biol. 2008;28(7):2257-70. Epub 20080122. doi: 10.1128/mcb.01755-07. PubMed PMID: 18212047; PubMed Central PMCID: PMCPMC2268442.
30. Utley RT, Ikeda K, Grant PA, Côté J, Steger DJ, Eberharter A, et al. Transcriptional activators direct histone acetyltransferase complexes to nucleosomes. Nature. 1998;394(6692):498-502. doi: 10.1038/28886. PubMed PMID: 9697775.
31. Cipollina C, Alberghina L, Porro D, Vai M. SFP1 is involved in cell size modulation in respiro-fermentative growth conditions. Yeast. 2005;22(5):385-99. doi: 10.1002/yea.1218. PubMed PMID: 15806610.
32. Jorgensen P, Nishikawa JL, Breitkreutz BJ, Tyers M. Systematic identification of pathways that couple cell growth and division in yeast. Science. 2002;297(5580):395-400. Epub 20020627. doi: 10.1126/science.1070850. PubMed PMID: 12089449.
33. Haruki H, Nishikawa J, Laemmli UK. The anchor-away technique: rapid, conditional establishment of yeast mutant phenotypes. Mol Cell. 2008;31(6):925-32. doi: 10.1016/j.molcel.2008.07.020. PubMed PMID: 18922474.
34. Zentner GE, Kasinathan S, Xin B, Rohs R, Henikoff S. ChEC-seq kinetics discriminates transcription factor binding sites by DNA sequence and shape in vivo. Nat Commun. 2015;6:8733. Epub 20151022. doi: 10.1038/ncomms9733. PubMed PMID: 26490019; PubMed Central PMCID: PMCPMC4618392.
35. Saleh MM, Tourigny JP, Zentner GE. Genome-Wide Profiling of Protein-DNA Interactions with Chromatin Endogenous Cleavage and High-Throughput Sequencing (ChEC-Seq). Methods Mol Biol. 2021;2351:289-303. doi: 10.1007/978-1-0716-1597-3_16. PubMed PMID: 34382196.
36. Slattery MG, Heideman W. Coordinated regulation of growth genes in Saccharomyces cerevisiae. Cell Cycle. 2007;6(10):1210-9. Epub 20070509. doi: 10.4161/cc.6.10.4257. PubMed PMID: 17495542.
37. Wade CH, Umbarger MA, McAlear MA. The budding yeast rRNA and ribosome biosynthesis (RRB) regulon contains over 200 genes. Yeast. 2006;23(4):293-306. doi: 10.1002/yea.1353. PubMed PMID: 16544271.
38. Rossi MJ, Lai WKM, Pugh BF. Genome-wide determinants of sequence-specific DNA binding of general regulatory factors. Genome Res. 2018;28(4):497-508. Epub 20180321. doi: 10.1101/gr.229518.117. PubMed PMID: 29563167; PubMed Central PMCID: PMCPMC5880240.
39. Bosio MC, Fermi B, Spagnoli G, Levati E, Rubbi L, Ferrari R, et al. Abf1 and other general regulatory factors control ribosome biogenesis gene expression in budding yeast. Nucleic Acids Res. 2017;45(8):4493-506. doi: 10.1093/nar/gkx058. PubMed PMID: 28158860; PubMed Central PMCID: PMCPMC5416754.
40. Brahma S, Henikoff S. CUT&RUN Profiling of the Budding Yeast Epigenome. Methods Mol Biol. 2022;2477:129-47. doi: 10.1007/978-1-0716-2257-5_9. PubMed PMID: 35524116.
41. Skene PJ, Henikoff S. An efficient targeted nuclease strategy for high-resolution mapping of DNA binding sites. Elife. 2017;6. Epub 20170116. doi: 10.7554/eLife.21856. PubMed PMID: 28079019; PubMed Central PMCID: PMCPMC5310842.

42. Zhang H, Roberts DN, Cairns BR. Genome-wide dynamics of Htz1, a histone H2A variant that poises repressed/basal promoters for activation through histone loss. Cell. 2005;123(2):219-31. doi: 10.1016/j.cell.2005.08.036. PubMed PMID: 16239141; PubMed Central PMCID: PMCPMC2788555.
43. Adam M, Robert F, Larochelle M, Gaudreau L. H2A.Z is required for global chromatin integrity and for recruitment of RNA polymerase II under specific conditions. Mol Cell Biol. 2001;21(18):6270-9. doi: 10.1128/MCB.21.18.6270-6279.2001. PubMed PMID: 11509669; PubMed Central PMCID: PMCPMC87352.
44. Fan JY, Rangasamy D, Luger K, Tremethick DJ. H2A.Z alters the nucleosome surface to promote HP1alpha-mediated chromatin fiber folding. Mol Cell. 2004;16(4):655-61. doi: 10.1016/j.molcel.2004.10.023. PubMed PMID: 15546624.
45. Cheng X, Auger A, Altaf M, Drouin S, Paquet E, Utley RT, et al. Eaf1 Links the NuA4 Histone Acetyltransferase Complex to Htz1 Incorporation and Regulation of Purine Biosynthesis. Eukaryot Cell. 2015;14(6):535-44. Epub 20150403. doi: 10.1128/ec.00004-15. PubMed PMID: 25841019; PubMed Central PMCID: PMCPMC4452573.
46. Altaf M, Auger A, Monnet-Saksouk J, Brodeur J, Piquet S, Cramet M, et al. NuA4-dependent acetylation of nucleosomal histones H4 and H2A directly stimulates incorporation of H2A.Z by the SWR1 complex. J Biol Chem. 2010;285(21):15966-77. Epub 20100323. doi: 10.1074/jbc.M110.117069. PubMed PMID: 20332092; PubMed Central PMCID: PMCPMC2871465.
47. Millar CB, Xu F, Zhang K, Grunstein M. Acetylation of H2AZ Lys 14 is associated with genome-wide gene activity in yeast. Genes Dev. 2006;20(6):711-22. doi: 10.1101/gad.1395506. PubMed PMID: 16543223; PubMed Central PMCID: PMCPMC1413291.
48. Gu M, Naiyachit Y, Wood TJ, Millar CB. H2A.Z marks antisense promoters and has positive effects on antisense transcript levels in budding yeast. BMC Genomics. 2015;16(1):99. Epub 20150219. doi: 10.1186/s12864-015-1247-4. PubMed PMID: 25765960; PubMed Central PMCID: PMCPMC4337092.
49. Knight B, Kubik S, Ghosh B, Bruzzone MJ, Geertz M, Martin V, et al. Two distinct promoter architectures centered on dynamic nucleosomes control ribosomal protein gene transcription. Genes Dev. 2014;28(15):1695-709. doi: 10.1101/gad.244434.114. PubMed PMID: 25085421; PubMed Central PMCID: PMCPMC4117944.
50. Reja R, Vinayachandran V, Ghosh S, Pugh BF. Molecular mechanisms of ribosomal protein gene coregulation. Genes Dev. 2015;29(18):1942-54. doi: 10.1101/gad.268896.115. PubMed PMID: 26385964; PubMed Central PMCID: PMCPMC4579351.
51. Zhu C, Byers KJ, McCord RP, Shi Z, Berger MF, Newburger DE, et al. High-resolution DNA-binding specificity analysis of yeast transcription factors. Genome Res. 2009;19(4):556-66. Epub 20090121. doi: 10.1101/gr.090233.108. PubMed PMID: 19158363; PubMed Central PMCID: PMCPMC2665775.
52. Sapountzi V, Côté J. MYST-family histone acetyltransferases: beyond chromatin. Cell Mol Life Sci. 2011;68(7):1147-56. Epub 20101204. doi: 10.1007/s00018-010-0599-9. PubMed PMID: 21132344; PubMed Central PMCID: PMCPMC11114825.
53. Carrozza MJ, Utley RT, Workman JL, Cote J. The diverse functions of histone acetyltransferase complexes. Trends Genet. 2003;19(6):321-9. doi: 10.1016/S0168-9525(03)00115-X. PubMed PMID: 12801725.

54. Lin YY, Lu JY, Zhang J, Walter W, Dang W, Wan J, et al. Protein acetylation microarray reveals that NuA4 controls key metabolic target regulating gluconeogenesis. Cell. 2009;136(6):1073-84. doi: 10.1016/j.cell.2009.01.033. PubMed PMID: 19303850; PubMed Central PMCID: PMCPMC2696288.
55. Yuan H, Rossetto D, Mellert H, Dang W, Srinivasan M, Johnson J, et al. MYST protein acetyltransferase activity requires active site lysine autoacetylation. Embo j. 2012;31(1):58-70. Epub 20111021. doi: 10.1038/emboj.2011.382. PubMed PMID: 22020126; PubMed Central PMCID: PMCPMC3252582.
56. Downey M, Johnson JR, Davey NE, Newton BW, Johnson TL, Galaang S, et al. Acetylome profiling reveals overlap in the regulation of diverse processes by sirtuins, gcn5, and esa1. Mol Cell Proteomics. 2015;14(1):162-76. Epub 20141107. doi: 10.1074/mcp.M114.043141. PubMed PMID: 25381059; PubMed Central PMCID: PMCPMC4288252.
57. Mameri A, Cote J. JAZF1: A metabolic actor subunit of the NuA4/TIP60 chromatin modifying complex. Front Cell Dev Biol. 2023;11:1134268. Epub 2023/04/24. doi: 10.3389/fcell.2023.1134268. PubMed PMID: 37091973; PubMed Central PMCID: PMC10119425.
58. Sudarshan D, Avvakumov N, Lalonde ME, Alerasool N, Joly-Beauparlant C, Jacquet K, et al. Recurrent chromosomal translocations in sarcomas create a megacomplex that mislocalizes NuA4/TIP60 to Polycomb target loci. Genes Dev. 2022;36(11-12):664-83. Epub 20220616. doi: 10.1101/gad.348982.121. PubMed PMID: 35710139; PubMed Central PMCID: PMCPMC9296003.
59. Procida T, Friedrich T, Jack APM, Peritore M, Bönisch C, Eberl HC, et al. JAZF1, A Novel p400/TIP60/NuA4 Complex Member, Regulates H2A.Z Acetylation at Regulatory Regions. Int J Mol Sci. 2021;22(2). Epub 20210112. doi: 10.3390/ijms22020678. PubMed PMID: 33445503; PubMed Central PMCID: PMCPMC7826843.
60. Cheng X, Côté V, Côté J. NuA4 and SAGA acetyltransferase complexes cooperate for repair of DNA breaks by homologous recombination. PLoS Genet. 2021;17(7):e1009459. Epub 20210706. doi: 10.1371/journal.pgen.1009459. PubMed PMID: 34228704; PubMed Central PMCID: PMCPMC8284799.
61. Allard S, Utley RT, Savard J, Clarke A, Grant P, Brandl CJ, et al. NuA4, an essential transcription adaptor/histone H4 acetyltransferase complex containing Esa1p and the ATM-related cofactor Tra1p. Embo j. 1999;18(18):5108-19. doi: 10.1093/emboj/18.18.5108. PubMed PMID: 10487762; PubMed Central PMCID: PMCPMC1171581.
62. Steunou AL, Cramet M, Rossetto D, Aristizabal MJ, Lacoste N, Drouin S, et al. Combined Action of Histone Reader Modules Regulates NuA4 Local Acetyltransferase Function but Not Its Recruitment on the Genome. Mol Cell Biol. 2016;36(22):2768-81. Epub 20161028. doi: 10.1128/mcb.00112-16. PubMed PMID: 27550811; PubMed Central PMCID: PMCPMC5086519.
63. Jacquet K, Fradet-Turcotte A, Avvakumov N, Lambert JP, Roques C, Pandita RK, et al. The TIP60 Complex Regulates Bivalent Chromatin Recognition by 53BP1 through Direct H4K20me Binding and H2AK15 Acetylation. Mol Cell. 2016;62(3):409-21. doi: 10.1016/j.molcel.2016.03.031. PubMed PMID: 27153538; PubMed Central PMCID: PMCPMC4887106.
64. Cheng X, Jobin-Robitaille O, Billon P, Buisson R, Niu H, Lacoste N, et al. Phospho-dependent recruitment of the yeast NuA4 acetyltransferase complex by MRX at DNA breaks regulates RPA dynamics during resection. Proc Natl Acad Sci U S A. 2018;115(40):10028-33.

Epub 20180917. doi: 10.1073/pnas.1806513115. PubMed PMID: 30224481; PubMed Central PMCID: PMCPMC6176631.
65. Chen S, Zhou Y, Chen Y, Gu J. fastp: an ultra-fast all-in-one FASTQ preprocessor. Bioinformatics. 2018;34(17):i884-i90. doi: 10.1093/bioinformatics/bty560. PubMed PMID: 30423086; PubMed Central PMCID: PMCPMC6129281.
66. Ewels P, Magnusson M, Lundin S, Käller M. MultiQC: summarize analysis results for multiple tools and samples in a single report. Bioinformatics. 2016;32(19):3047-8. Epub 20160616. doi: 10.1093/bioinformatics/btw354. PubMed PMID: 27312411; PubMed Central PMCID: PMCPMC5039924.
67. Bray NL, Pimentel H, Melsted P, Pachter L. Near-optimal probabilistic RNA-seq quantification. Nat Biotechnol. 2016;34(5):525-7. Epub 20160404. doi: 10.1038/nbt.3519. PubMed PMID: 27043002.
68. Lê S, Josse J, Husson F. FactoMineR: An R Package for Multivariate Analysis. Journal of Statistical Software. 2008;25(1):1 - 18. doi: 10.18637/jss.v025.i01.
69. Wickham H. ggplot2. WIREs Computational Statistics. 2011;3(2):180-5. doi: https://doi.org/10.1002/wics.147.
70. Love MI, Huber W, Anders S. Moderated estimation of fold change and dispersion for RNA-seq data with DESeq2. Genome Biol. 2014;15(12):550. doi: 10.1186/s13059-014-0550-8. PubMed PMID: 25516281; PubMed Central PMCID: PMCPMC4302049.
71. Yu G, Wang LG, He QY. ChIPseeker: an R/Bioconductor package for ChIP peak annotation, comparison and visualization. Bioinformatics. 2015;31(14):2382-3. Epub 20150311. doi: 10.1093/bioinformatics/btv145. PubMed PMID: 25765347.
72. Gu Z, Eils R, Schlesner M. Complex heatmaps reveal patterns and correlations in multidimensional genomic data. Bioinformatics. 2016;32(18):2847-9. Epub 20160520. doi: 10.1093/bioinformatics/btw313. PubMed PMID: 27207943.
73. Orsi GA, Kasinathan S, Zentner GE, Henikoff S, Ahmad K. Mapping regulatory factors by immunoprecipitation from native chromatin. Curr Protoc Mol Biol. 2015;110:21.31.1-21.31.25. Epub 20150401. doi: 10.1002/0471142727.mb2131s110. PubMed PMID: 25827087; PubMed Central PMCID: PMCPMC4410783.
74. Li H. Aligning sequence reads, clone sequences and assembly contigs with BWA-MEM. arXiv preprint arXiv:13033997. 2013.
75. Li H, Handsaker B, Wysoker A, Fennell T, Ruan J, Homer N, et al. The Sequence Alignment/Map format and SAMtools. Bioinformatics. 2009;25(16):2078-9. Epub 20090608. doi: 10.1093/bioinformatics/btp352. PubMed PMID: 19505943; PubMed Central PMCID: PMCPMC2723002.
76. Feng J, Liu T, Qin B, Zhang Y, Liu XS. Identifying ChIP-seq enrichment using MACS. Nat Protoc. 2012;7(9):1728-40. Epub 20120830. doi: 10.1038/nprot.2012.101. PubMed PMID: 22936215; PubMed Central PMCID: PMCPMC3868217.
77. Ramírez F, Dündar F, Diehl S, Grüning BA, Manke T. deepTools: a flexible platform for exploring deep-sequencing data. Nucleic Acids Res. 2014;42(Web Server issue):W187-91. Epub 20140505. doi: 10.1093/nar/gku365. PubMed PMID: 24799436; PubMed Central PMCID: PMCPMC4086134.

78. Quinlan AR, Hall IM. BEDTools: a flexible suite of utilities for comparing genomic features. Bioinformatics. 2010;26(6):841-2. Epub 20100128. doi: 10.1093/bioinformatics/btq033. PubMed PMID: 20110278; PubMed Central PMCID: PMCPMC2832824.
79. Kent WJ, Zweig AS, Barber G, Hinrichs AS, Karolchik D. BigWig and BigBed: enabling browsing of large distributed datasets. Bioinformatics. 2010;26(17):2204-7. Epub 20100717. doi: 10.1093/bioinformatics/btq351. PubMed PMID: 20639541; PubMed Central PMCID: PMCPMC2922891.
80. Robinson JT, Thorvaldsdóttir H, Winckler W, Guttman M, Lander ES, Getz G, et al. Integrative genomics viewer. Nat Biotechnol. 2011;29(1):24-6. doi: 10.1038/nbt.1754. PubMed PMID: 21221095; PubMed Central PMCID: PMCPMC3346182.
81. Gu Z, Eils R, Schlesner M, Ishaque N. EnrichedHeatmap: an R/Bioconductor package for comprehensive visualization of genomic signal associations. BMC Genomics. 2018;19(1):234. Epub 20180404. doi: 10.1186/s12864-018-4625-x. PubMed PMID: 29618320; PubMed Central PMCID: PMCPMC5885322.
82. Khan A, Mathelier A. Intervene: a tool for intersection and visualization of multiple gene or genomic region sets. BMC Bioinformatics. 2017;18(1):287. Epub 20170531. doi: 10.1186/s12859-017-1708-7. PubMed PMID: 28569135; PubMed Central PMCID: PMCPMC5452382.

Figure Legends

Figure 1. Sfp1 interacts with NuA4 in vivo and in vitro. A) Western blots of Tra1, a subunit of NuA4 complex, detected from Sfp1-TAP and Epl1-TAP purified complexes. **B)** Western blots of Eaf1 and Arp4, selected subunits of the NuA4 complex, confirm the interaction between Sfp1 and NuA4 complex in vivo. **C)** Sfp1 interacts with NuA4 in vitro in a rapamycin-independent manner. Lysates from yeasts expressing Sfp1-Myc and/or Epl1-FLAG were subjected to immunoprecipitation using anti-Myc antibody, and eluted proteins were analyzed by western blots using the antibody against Flag. For indicated samples, cells were treated with rapamycin (200ng/mL) for 2 hours to inhibit TOR kinase. **D)** TAP-purified NuA4 complex was incubated with recombinant Sfp1 or GCN4 protein on glutathione magnetic beads. In vitro histone acetyltransferase (HAT) assay was performed with Sfp1-bonded NuA4. The NuA4 in the supernatant after incubation served as a control.

Figure 2. Rapamycin-induced Sfp1 depletion does not affect NuA4 recruitment on RP gene promoters. A) FRB tagging of *SFP1* was constructed in rapamycin-resistant parental strain to induce Sfp1 depletion employing anchor-away (AA). Rapamycin (1 µg/mL) was used to trigger AA depletion. Sfp1-depleted cells show growth defects on rapamycin agar plates whereas no-FRB control cells grow normally. **B-C)** Mislocalization of Sfp1 at RPL2B and RPS11B gene promoters determined by ChIP-qPCR using anti-FRB antibody**.** Sfp1-FRB cells were treated with rapamycin (1 µg/mL) for 2 hours. An isogenic no-FRB strain was used as a negative control. **D)** NuA4 recruitment at RP gene promoters upon Sfp1 depletion was determined by ChIP-qPCR with anti-Eaf1 antibody. Error bars represent the range of two independent experiments.

Figure 3. NuA4 binding at the ribosomal protein (RP) gene and ribosome biogenesis (RiBi) gene promoters are not affected by Sfp1 depletion. A) IGV tracks showing Eaf1 CUT&RUN peaks at RiBi (*HAS1*) and RP (*RPS11B*) gene promoters in Sfp1 nuclear-depleted cells. IgG control tracks were subtracted from normalized RPM tracks. **B)** Box plots showing Eaf1 binding upon Sfp1 depletion at the promoters of different gene clusters (Ribosomal protein (RP) genes, Ribosome Biogenesis (RiBi) genes, Ribosome Biogenesis like (RiBi-like) genes). Samples with or without Sfp1 were coloured in marron and indigo, respectively. Box plots were computed using means of bins per gene. The *p*-value was calculated by Wilcoxon testing.

Figure 4. Sfp1 depletion attenuates H3 and H4 acetylation while occupancy of histone variant Htz1 shows an increase at RiBi and RiBi-like gene promoters. A) Box plots showing genome-wide histone acetylation change and Htz1 occupancy change upon Sfp1 depletion measured by ChIP-seq. Tracks were normalized to histone H3 levels and are from biological replicates. **C)** Htz1 acetylation is decreased in Sfp1-depleted cells. Immunoprecipitations (IP) were performed with whole cell extracts from cells with or without Sfp1 using an anti-acetyl-lysine antibody. Htz1, H4 and H3 acetylation levels were determined by western blotting. **D-F)** ChIP-qPCR of Htz1.K14ac changes at selected RP (*RPS11B*) and RiBi (*NOB1* and *NSA1*) gene promoters upon Sfp1 depletion. Values are a ratio of IP/input of Htz1.K14ac vs Htz1. Error bars represent the range of two independent experiments.

Figure 5. Esa1 depletion affects Sfp1 binding at specific ribosomal protein gene promoters. A) FRB tagging of *Esa1* was constructed in rapamycin-resistant parental strain to induce Esa1 depletion by means of anchor-away (AA). FRB was tagged at the N-terminus of Esa1 to avoid

impeding its function. Rapamycin (1 µg/mL) is used to trigger AA depletion. Esa1-depleted cells show growth defects on rapamycin agar plates while no-FRB control cells grow normally. **B)** H4 acetylation changes were measured by western blotting upon Esa1 depletion. The anti-H4ac antibody recognizes H2A acetylation non-specifically. Anti-H3 was used as a control of the amount of total histone H3. **C)** ChIP-qPCR of H4K8ac showed a decreased level at RP (*RPL2B* and *RPS11B*) and RiBi (*NOB1* and *HAS1*) gene promoters upon Esa1 depletion. Values are a ratio of the percentage input of H4K8ac and H3. Error bars represent the standard error of three independent experiments. **D)** Box plots showing Sfp1 enrichment determined by CUT&RUN at different gene clusters upon Esa1 depletion. **E)** Box plots showing Sfp1 binding at different categories of RP gene promoters upon Esa1 depletion. Box plots were computed using means of bins per gene **F)** IGV tracks showing Sfp1 CUT&RUN peaks at different categories of RP gene promoters upon Esa1 depletion. Category I (*RPL2B* and *RPS11B*), Category II (*RPL23A* and *RPS2*), Category III (*RPS21A* and *RPL1A*). IgG controls were subtracted from normalized RPM tracks.

Figure 6. Esa1-dependent Sfp1 Lysine 655 and 657 acetylation affects its binding at target genes in normal and TOR-inhibited conditions. A) Diagram showing the location of the lysine residues acetylated by Esa1 and predicted Zinc-finger domains of Sfp1. **B)** Sfp1 acetylation is regulated by sirtuins. Myc-tagged Sfp1 was Immunoprecipitated from wild-type or *sir2*Δ *hst1*Δ *hst2*Δ (ΔHDACs) triple mutant and analyzed with an antibody directed towards acetylated lysine or the myc epitope. The acetylation status was compared between wild-type Sfp1 and Sfp1 with lysine K655 and K657 mutated to arginine (wt vs R) by western blotting. **C)** Spot assay testing growth rates of wild-type cells and Sfp1 mutants in YPD and Tor-inhibited conditions. Ten-fold serial dilutions of strain expression indicated Sfp1 on complete media or complete media

containing rapamycin (200µg/mL). **D)** ΔHDACs cells were hypersensitive to rapamycin. Sfp1 K655/657 mutants were introduced in *sir2*Δ *hst1*Δ *hst2*Δ (ΔHDACs) triple mutated strain. Spot assay conditions are the same as in C). **E)** IGV tracks showing Sfp1 CUT&RUN peaks at selected RiBi (HAS1) and RP (RPL2B) gene promoters. IgG was subtracted from normalized RPM tracks. Wild-type Sfp1 coloured in marron, K655/657Q mutant coloured in indigo. **F-G)** Box plots showing Sfp1 and Eaf1 CUT&RUN signals at different gene clusters. The wild-type and K655/657Q mutant strains were compared in normal YPD and TOR-inhibited (200µg/mL rapamycin) conditions. Box plots and associated Wilcoxon tests were computed using means of bins per gene.

Figure 7. Sfp1 K655 and K657 acetylation upregulate RiBi gene expression under normal growth conditions. A) RNAs were extracted from log phase wild-type Sfp1, K655/657R, and K655/657Q strains growing in YPD. mRNA level of indicated RiBi genes (*NOB1*, *HAS1*, *NUG1*, *RPF2* and *NSA1*) and RP genes (*RPL2B* and *RPS11B*) were quantified, relative to levels of *ACT1* mRNA, by qPCR analysis. Error bars represent the range of two independent experiments. **B)** Volcano plot of differential gene expression analysis of Sfp1-K655/657Q mutant strain compared with wild-type strain. RiBi genes were highlighted in orange. Genes were considered significantly dysregulated for absolute fold change ratio >=1.5 and adjusted p-value <0.05. **C)** Box plots showing gene expression changes of different clusters (RiBi, RiBi-like, and RP genes) in K655/657Q mutant compared with wild-type cells growing in YPD. **D)** Heatmap showing differential gene expression of wild-type strain compared with acetyl-mimic Sfp1 strain.

Figure 8. K655/657Q mutations in Sfp1 provoke sensitivity to carbon shift from glucose to raffinose. A) Cells expressing indicated Sfp1 and its mutations were grown in YPD to log phase before transferred into media that contains raffinose as a single carbon source. mRNA level of indicated RiBi genes (*NOB1*, *HAS1*, *NUG1*, *RPF2* and *NSA1*) and RP genes (*RPL2B* and *RPS11B*) were quantified, relative to levels of *ACT1* mRNA, by qPCR analysis. Error bars represent the range of two independent experiments. **B)** Volcano plot of differential gene expression analysis of Sfp1-K655/657Q mutant strain compared with wild-type strain grown in raffinose. RiBi genes were highlighted in orange. Genes were considered significantly dysregulated for absolute fold change ratio >=1.5 and adjusted p-value <0.05. **C)** Box plots showing gene expression changes between different clusters (RiBi, RiBi-like, and RP genes) in K655/657Q mutant compared with wild-type cells grown in raffinose. **D)** Heatmap showing differential gene expression in raffinose of wild-type strain compared with acetyl-mimic Sfp1 strain.

Figure 9. NuA4-dependent acetylation of Sfp1 regulates RP gene transcription differentially from RiBi gene transcription upon carbon source shift followed by glucose pules. A) Flow diagram of carbon shift assay. Wild-type and Sfp1 mutants were grown in raffinose prior to the addition of glucose. Cells were collected at different time points for RNA quantifications. **B-C)** RNAs were extracted from log phase wild-type Sfp1, K655/657R, and K655/657Q strains growing in indicated media. Gene expression levels of selected RP genes (*RPL2B* and *RPS11B*) were quantified, relative to levels of *ACT1* mRNA, by RT-qPCR. Values at time 0 were normalized to 1. Error bars represent the range of two independent experiments. **D-E)** Gene expression levels of selected RiBi genes (NOB1 and HAS1) were quantified by RT-qPCR. Values at time 0 were normalized to 1. **F-G)** Box plots showing gene expression changes among carbon

shifts comparing the wild-type strain and Sfp1 mutants, determined by RNA-seq. At 15min and 30min, glucose was added back into the media for the indicated times. Values were normalized to time 0 respectively. RiBi and RP gene clusters were shown separately.

Figure 10. Interplay of NuA4 and Sfp1 at RP and RiBi genes. A) In rich media Sfp1 is not involved in NuA4 recruitment but affects its acetyltransferase function at RiBi/RP gene promoters. In parallel, NuA4 stimulates the binding of Sfp1 at RP gene promoters. **B)** Mimicking constitutive acetylation of Sfp1 by NuA4 stimulates its binding to RiBi genes in rich media but is detrimental in stress/poor carbon source conditions.

Figure 1

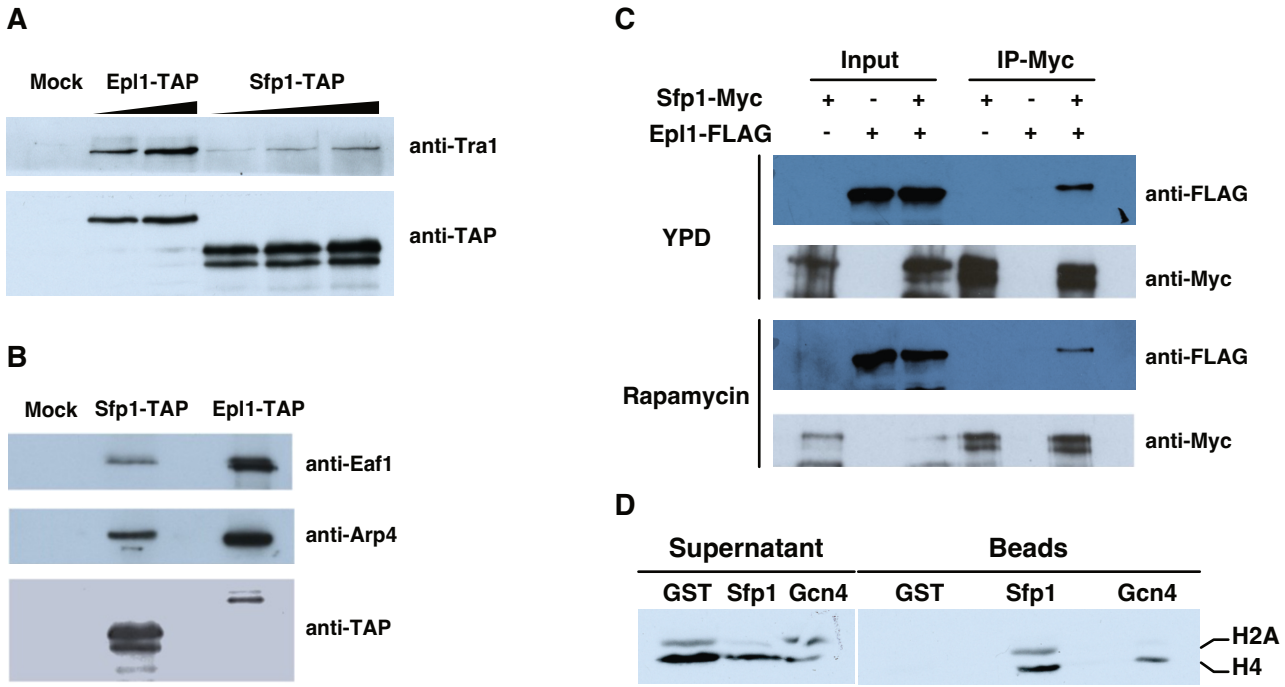
A
Mock
Epl1-TAP
Sfp1-TAP
anti-Tra1
anti-TAP
B
Mock
Sfp1-TAP
Epl1-TAP
anti-Eaf1
anti-Arp4
anti-TAP
C
Input
IP-Myc
Sfp1-Myc
+ - + + - +
Epl1-FLAG
- + + - + +
YPD
anti-FLAG
anti-Myc
Rapamycin
anti-FLAG
anti-Myc
D
Supernatant
Beads
GST Sfp1 Gcn4
GST Sfp1 Gcn4
H2A
H4

Figure 2

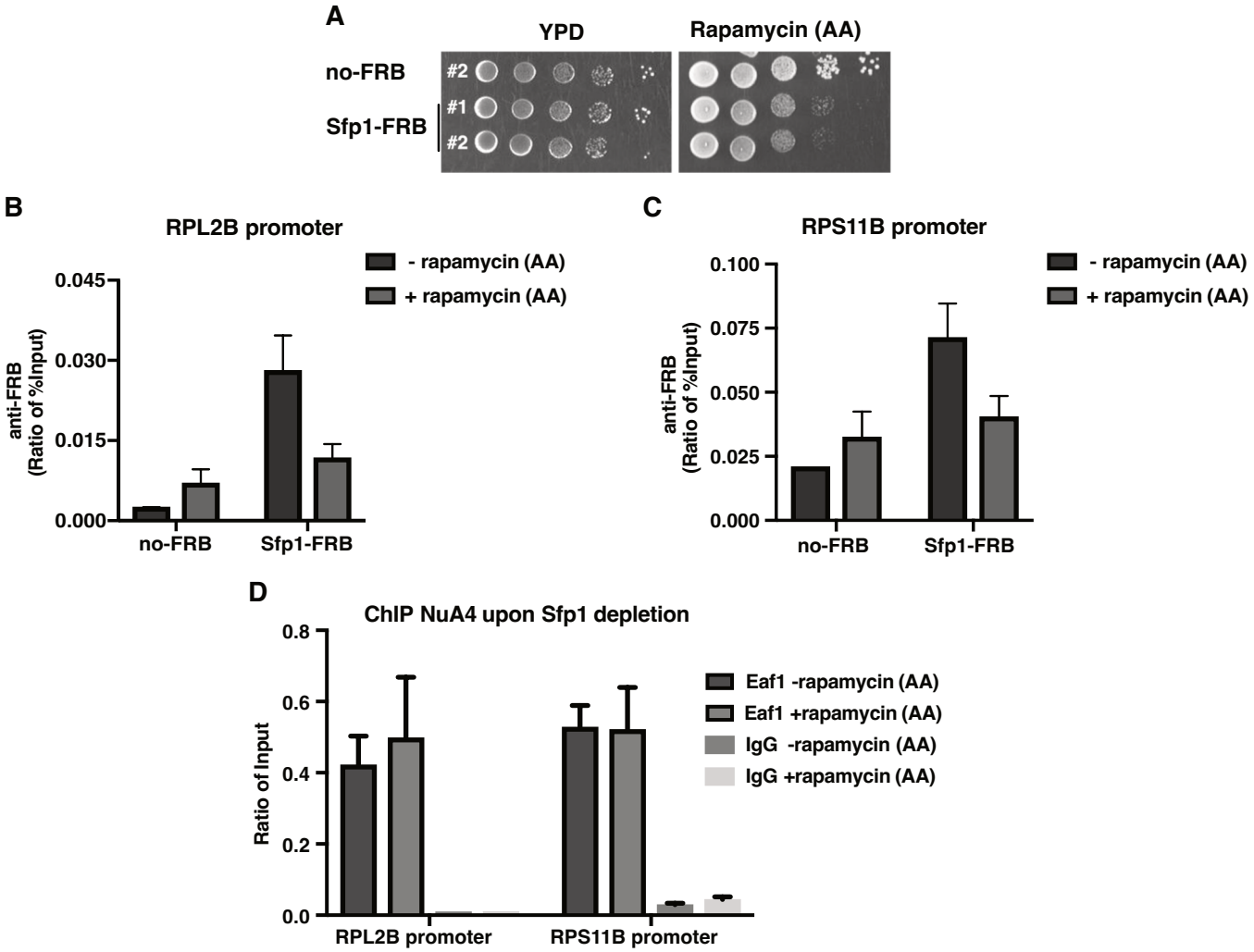
A
YPD
Rapamycin (AA)
no-FRB
Sfp1-FRB
#2
#1
#2
B
RPL2B promoter
- rapamycin (AA)
+ rapamycin (AA)
anti-FRB
(Ratio of %Input)
0.045
0.030
0.015
0.000
no-FRB
Sfp1-FRB
C
RPS11B promoter
- rapamycin (AA)
+ rapamycin (AA)
anti-FRB
(Ratio of %Input)
0.100
0.075
0.050
0.025
0.000
no-FRB
Sfp1-FRB
D
ChIP NuA4 upon Sfp1 depletion
Ratio of Input
0.8
0.6
0.4
0.2
0.0
Eaf1 -rapamycin (AA)
Eaf1 +rapamycin (AA)
IgG -rapamycin (AA)
IgG +rapamycin (AA)
RPL2B promoter
RPS11B promoter

Figure 3

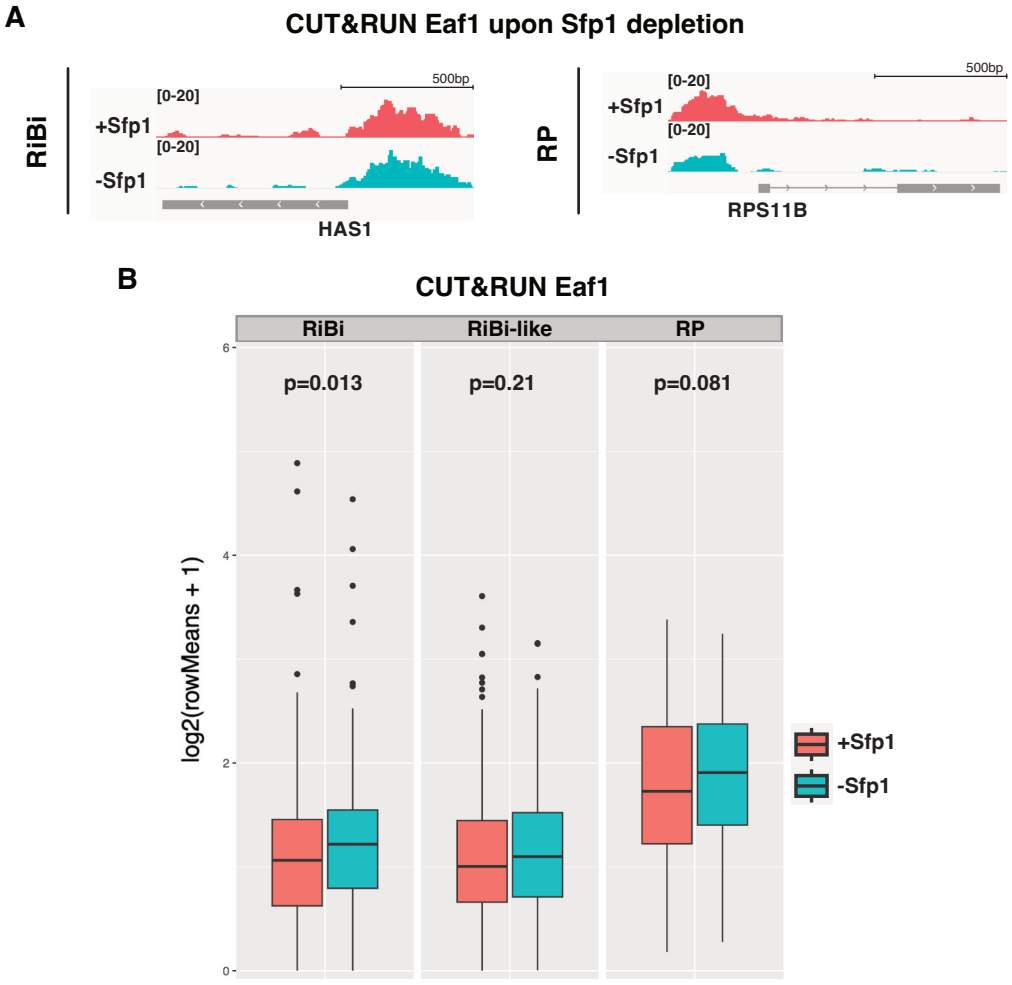
A
CUT&RUN Eaf1 upon Sfp1 depletion
RiBi
+Sfp1
-Sfp1
[0-20]
[0-20]
500bp
HAS1
RP
+Sfp1
-Sfp1
[0-20]
[0-20]
500bp
RPS11B
B
CUT&RUN Eaf1
RiBi
RiBi-like
RP
p=0.013
p=0.21
p=0.081
log2(rowMeans + 1)
0
2
4
6
+Sfp1
-Sfp1

Figure 4

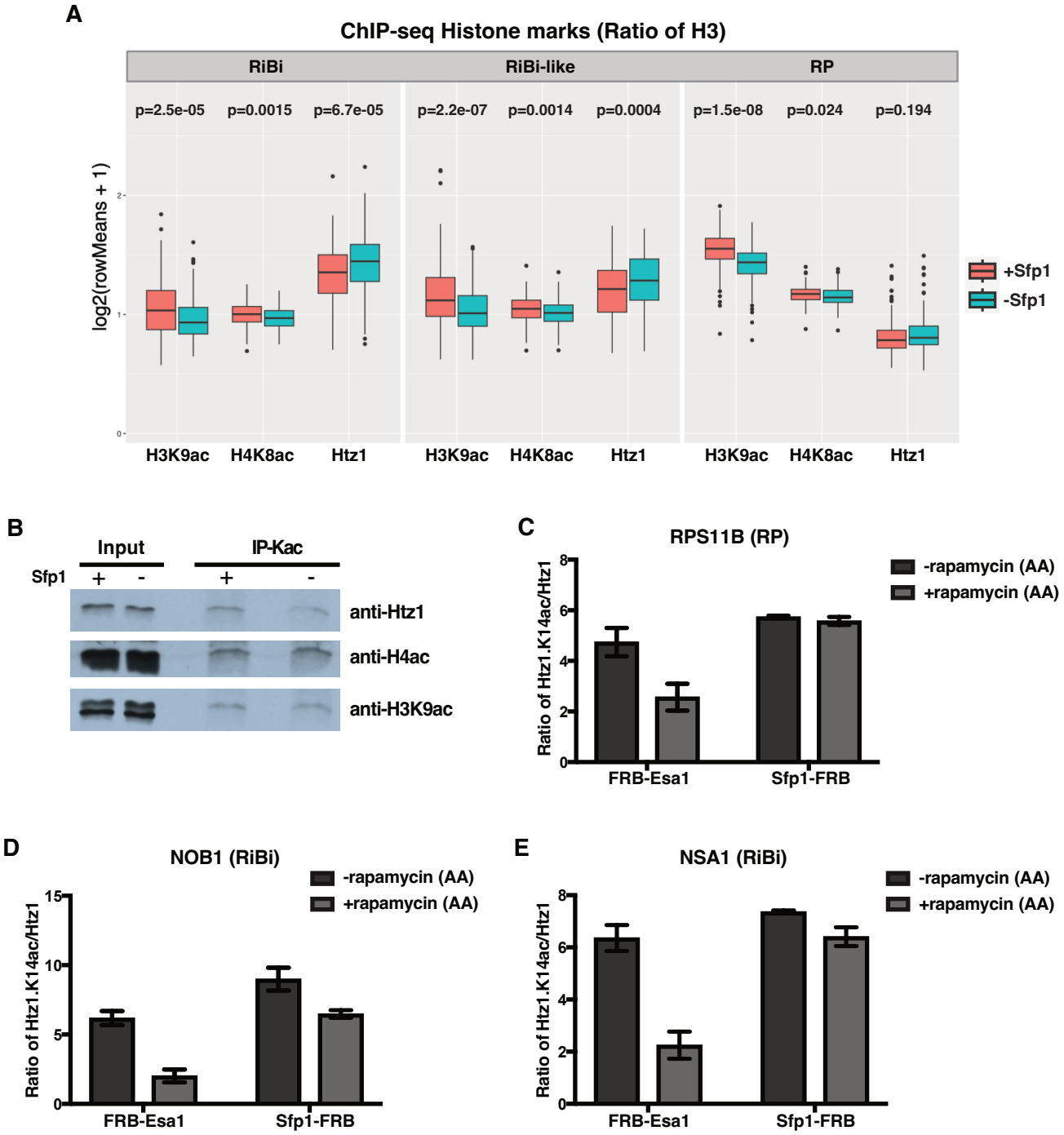
A
ChIP-seq Histone marks (Ratio of H3)
RiBi
RiBi-like
RP
p=2.5e-05
p=0.0015
p=6.7e-05
p=2.2e-07
p=0.0014
p=0.0004
p=1.5e-08
p=0.024
p=0.194
log2(rowMeans + 1)
H3K9ac
H4K8ac
Htz1
+Sfp1
-Sfp1
B
Input
IP-Kac
Sfp1
+
-
+
-
anti-Htz1
anti-H4ac
anti-H3K9ac
C
RPS11B (RP)
Ratio of Htz1.K14ac/Htz1
-rapamycin (AA)
+rapamycin (AA)
FRB-Esa1
Sfp1-FRB
D
NOB1 (RiBi)
Ratio of Htz1.K14ac/Htz1
-rapamycin (AA)
+rapamycin (AA)
FRB-Esa1
Sfp1-FRB
E
NSA1 (RiBi)
Ratio of Htz1.K14ac/Htz1
-rapamycin (AA)
+rapamycin (AA)
FRB-Esa1
Sfp1-FRB

Figure 5

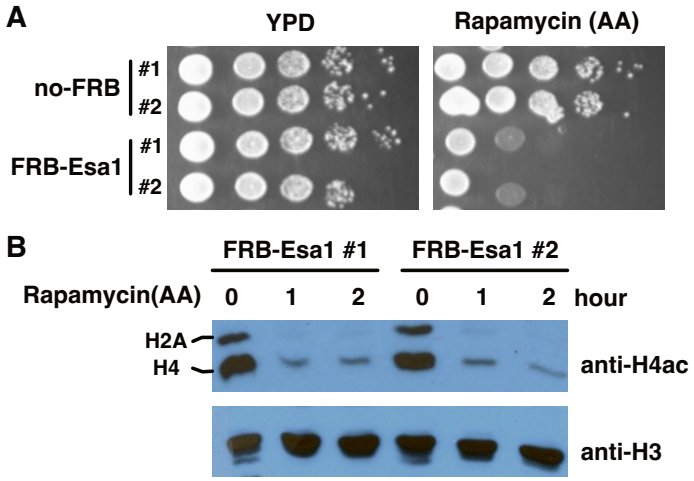
A
YPD
Rapamycin (AA)
no-FRB
#1
#2
FRB-Esa1
#1
#2
B
FRB-Esa1 #1
FRB-Esa1 #2
Rapamycin(AA)
0
1
2
0
1
2
hour
H2A
H4
anti-H4ac
anti-H3

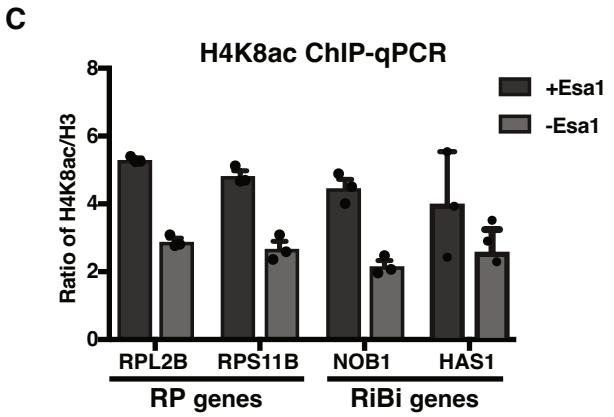
C
H4K8ac ChIP-qPCR
+Esa1
-Esa1
Ratio of H4K8ac/H3
0
2
4
6
8
RPL2B
RPS11B
NOB1
HAS1
RP genes
RiBi genes

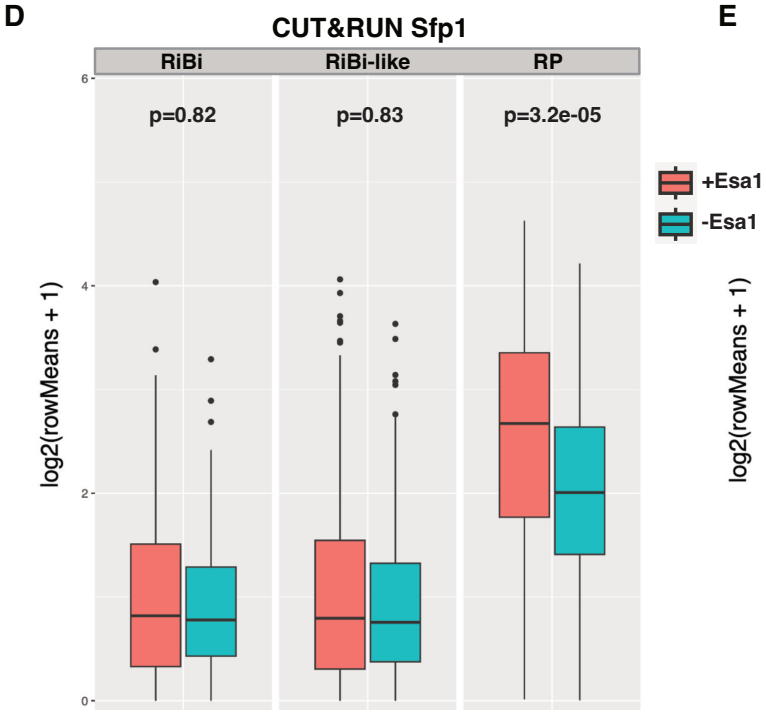
D
CUT&RUN Sfp1
RiBi
RiBi-like
RP
p=0.82
p=0.83
p=3.2e-05
+Esa1
-Esa1
log2(rowMeans + 1)
0
2
4
6

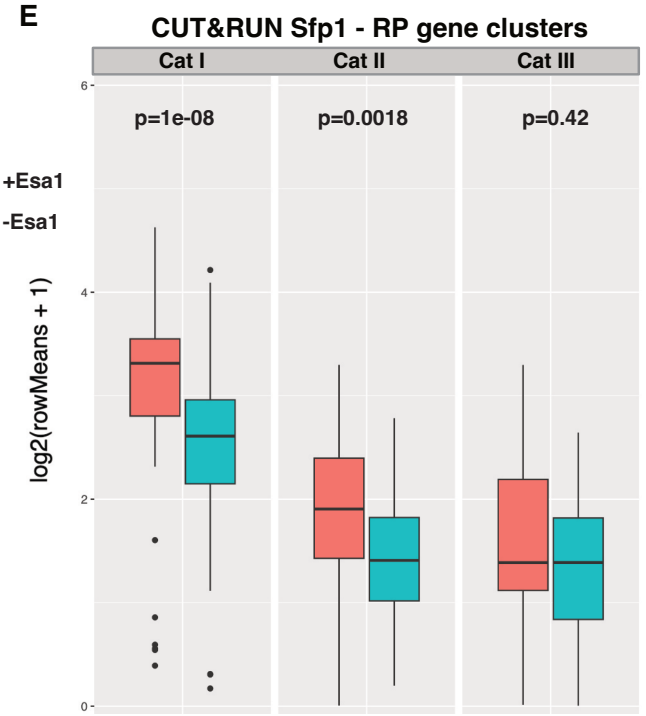
E
CUT&RUN Sfp1 - RP gene clusters
Cat I
Cat II
Cat III
p=1e-08
p=0.0018
p=0.42
log2(rowMeans + 1)
0
2
4
6

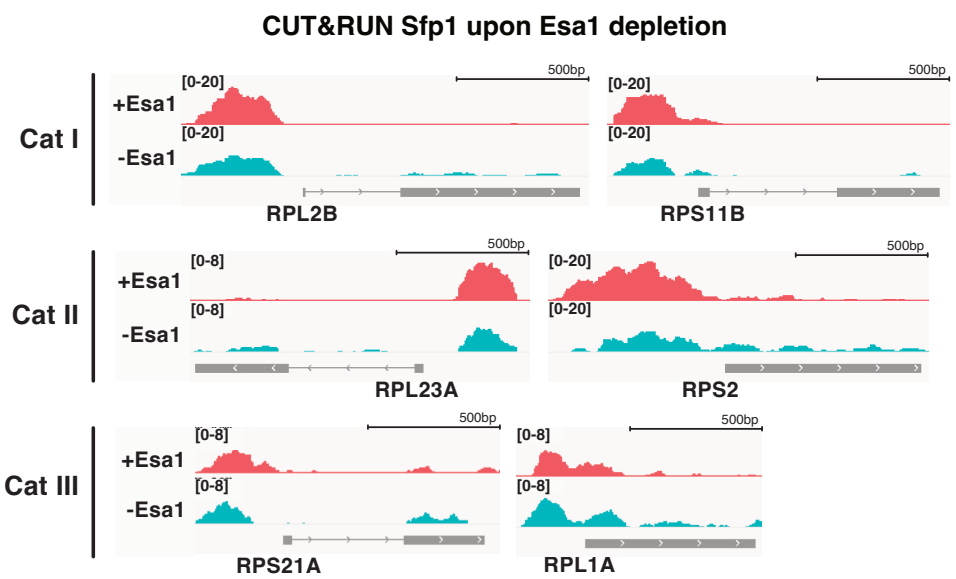
F
CUT&RUN Sfp1 upon Esa1 depletion
Cat I
+Esa1
-Esa1
[0-20]
500bp
RPL2B
RPS11B
Cat II
[0-8]
[0-20]
RPL23A
RPS2
Cat III
RPS21A
RPL1A

Figure 6

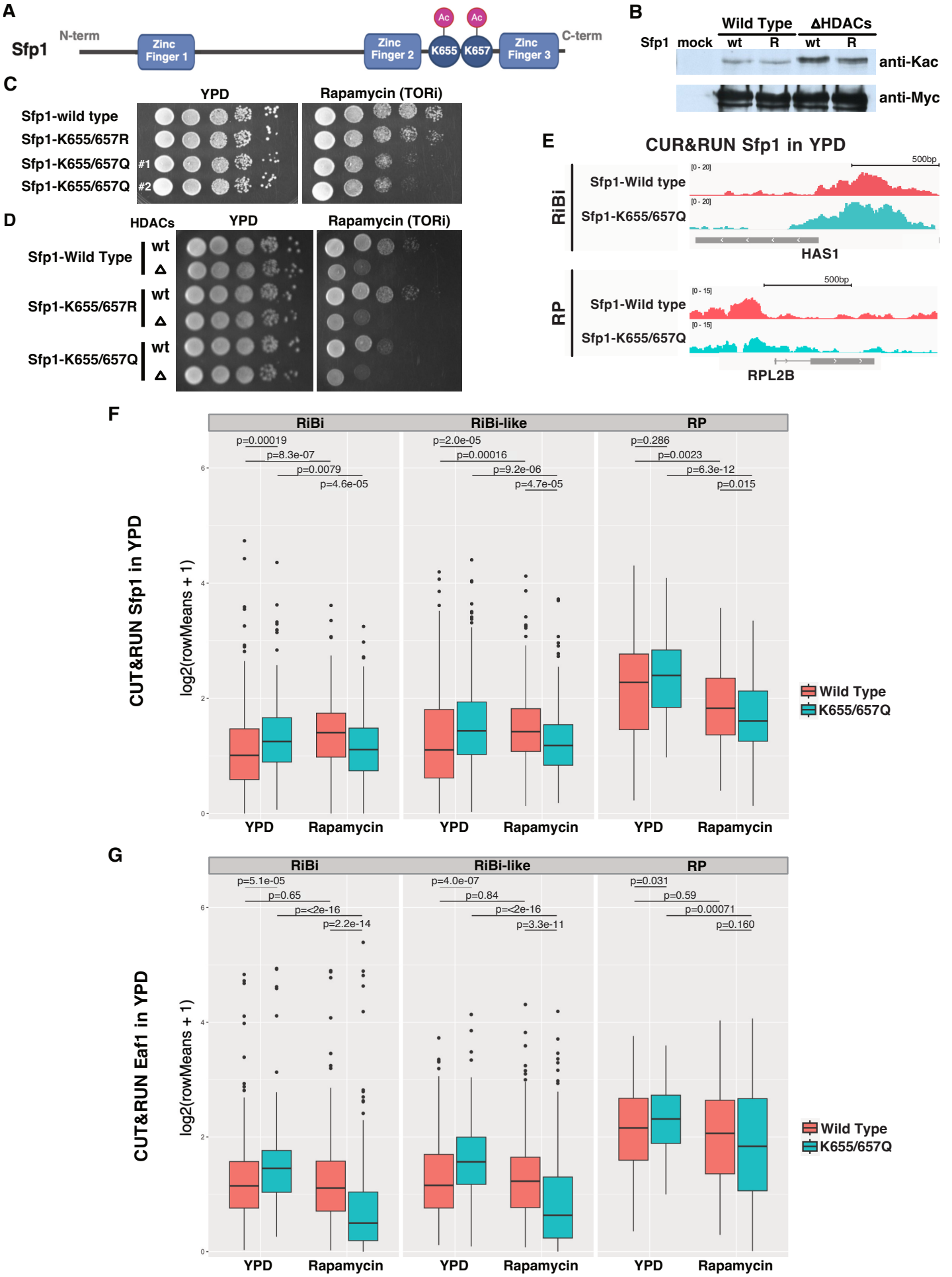
A
Sfp1
N-term
Zinc Finger 1
Zinc Finger 2
Ac
Ac
K655
K657
Zinc Finger 3
C-term
B
Wild Type
ΔHDACs
Sfp1 mock wt R wt R
anti-Kac
anti-Myc
C
YPD
Rapamycin (TORi)
Sfp1-wild type
Sfp1-K655/657R
Sfp1-K655/657Q #1
Sfp1-K655/657Q #2
D
HDACs
YPD
Rapamycin (TORi)
Sfp1-Wild Type wt Δ
Sfp1-K655/657R wt Δ
Sfp1-K655/657Q wt Δ
E
CUR&RUN Sfp1 in YPD
RiBi
Sfp1-Wild type
Sfp1-K655/657Q
500bp
HAS1
RP
Sfp1-Wild type
Sfp1-K655/657Q
500bp
RPL2B
F
CUT&RUN Sfp1 in YPD
log2(rowMeans + 1)
RiBi
RiBi-like
RP
p=0.00019
p=8.3e-07
p=0.0079
p=4.6e-05
p=2.0e-05
p=0.00016
p=9.2e-06
p=4.7e-05
p=0.286
p=0.0023
p=6.3e-12
p=0.015
YPD
Rapamycin
Wild Type
K655/657Q
G
CUT&RUN Eaf1 in YPD
log2(rowMeans + 1)
RiBi
RiBi-like
RP
p=5.1e-05
p=0.65
p=<2e-16
p=2.2e-14
p=4.0e-07
p=0.84
p=<2e-16
p=3.3e-11
p=0.031
p=0.59
p=0.00071
p=0.160
YPD
Rapamycin
Wild Type
K655/657Q

Figure 7

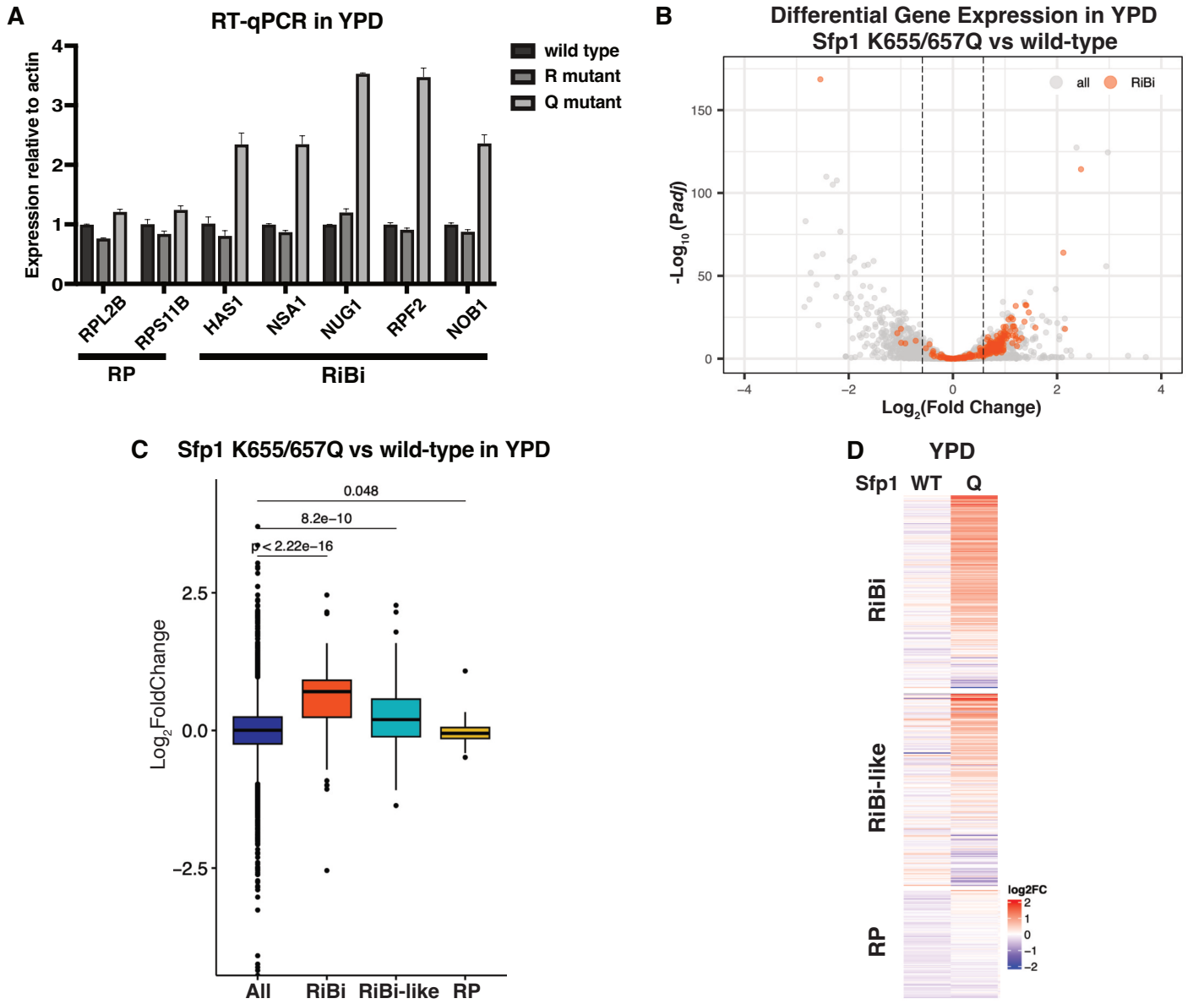
A
RT-qPCR in YPD
Expression relative to actin
wild type
R mutant
Q mutant
RPL2B
RPS11B
HAS1
NSA1
NUG1
RPF2
NOB1
RP
RiBi
B
Differential Gene Expression in YPD
Sfp1 K655/657Q vs wild-type
all
RiBi
-Log10 (Padj)
Log2(Fold Change)
C
Sfp1 K655/657Q vs wild-type in YPD
0.048
8.2e−10
p < 2.22e−16
Log2FoldChange
All
RiBi
RiBi-like
RP
D
YPD
Sfp1
WT
Q
RiBi
RiBi-like
RP
log2FC

Figure 8

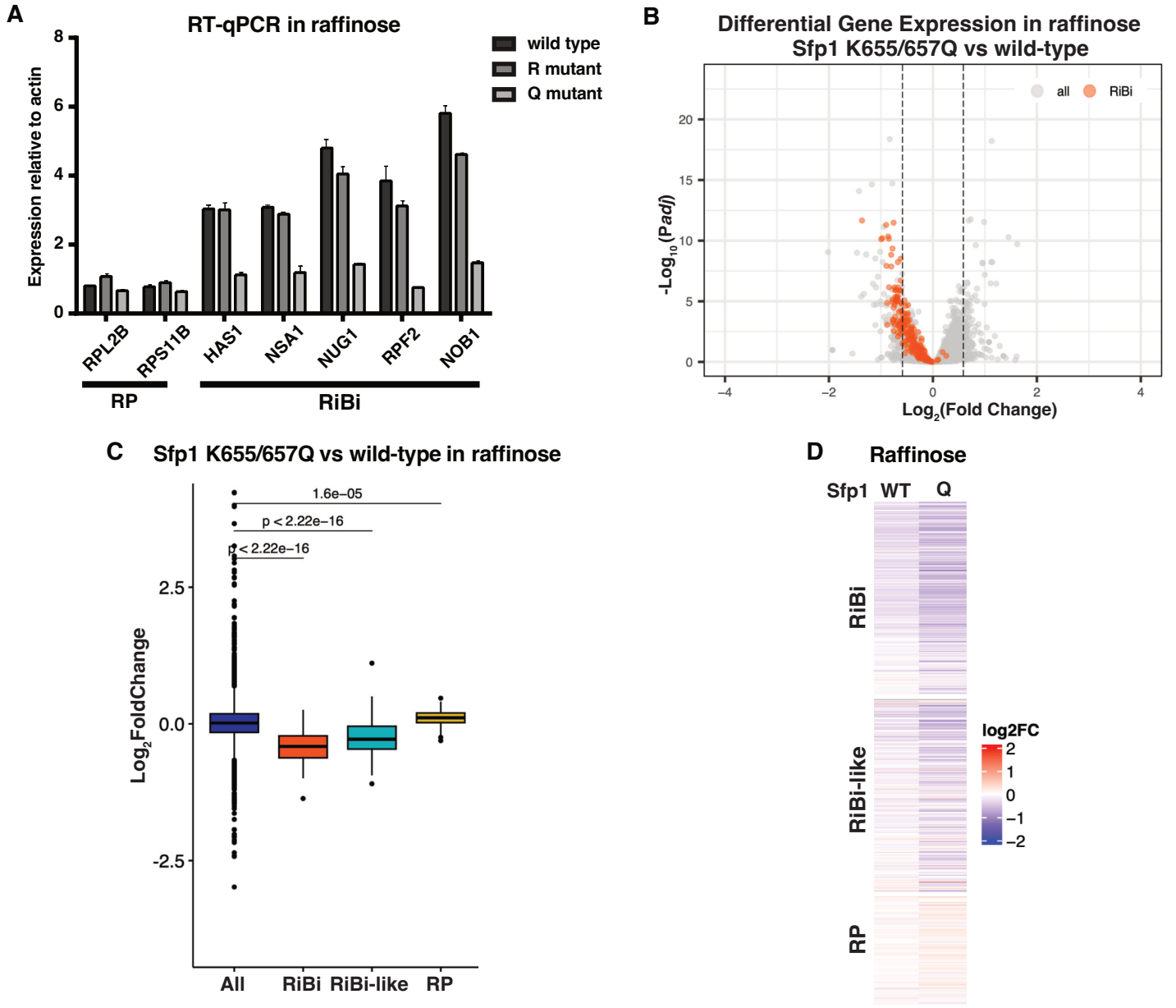
A
RT-qPCR in raffinose
Expression relative to actin
wild type
R mutant
Q mutant
RPL2B
RPS11B
HAS1
NSA1
NUG1
RPF2
NOB1
RP
RiBi
B
Differential Gene Expression in raffinose
Sfp1 K655/657Q vs wild-type
all
RiBi
-Log10 (Padj)
Log2(Fold Change)
C
Sfp1 K655/657Q vs wild-type in raffinose
1.6e−05
p < 2.22e−16
p < 2.22e−16
Log2FoldChange
All
RiBi
RiBi-like
RP
D
Raffinose
Sfp1
WT
Q
RiBi
RiBi-like
RP
log2FC

Figure 9

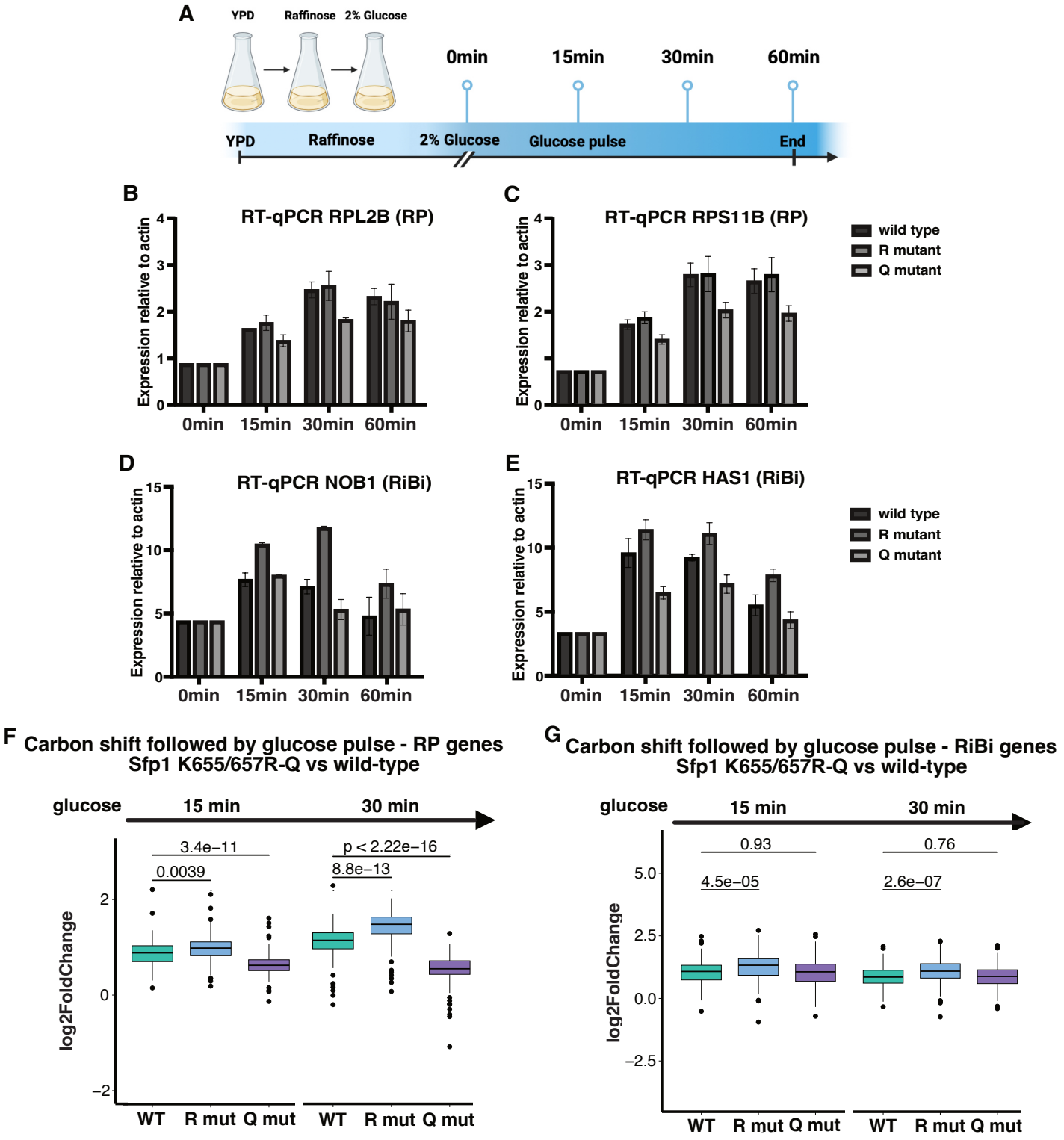
A
YPD
Raffinose
2% Glucose
0min
15min
30min
60min
YPD
Raffinose
2% Glucose
Glucose pulse
End
B
RT-qPCR RPL2B (RP)
Expression relative to actin
0min 15min 30min 60min
C
RT-qPCR RPS11B (RP)
wild type
R mutant
Q mutant
D
RT-qPCR NOB1 (RiBi)
E
RT-qPCR HAS1 (RiBi)
F
Carbon shift followed by glucose pulse - RP genes
Sfp1 K655/657R-Q vs wild-type
glucose
15 min
30 min
3.4e−11
0.0039
p < 2.22e−16
8.8e−13
log2FoldChange
WT R mut Q mut
G
Carbon shift followed by glucose pulse - RiBi genes
Sfp1 K655/657R-Q vs wild-type
0.93
4.5e−05
0.76
2.6e−07

Figure 10

A

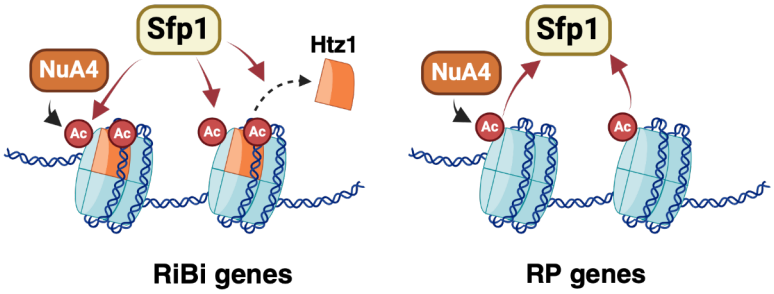
Sfp1
NuA4
Htz1
Ac
Ac
Ac
Ac
RiBi genes
Sfp1
NuA4
Ac
Ac
RP genes

B

In YPD
In Raffinose / TOR inhibition
NuA4
Sfp1
Q
Q
RiBi
Sfp1
Q
Q
RiBi

Supporting information

S1 Fig. NuA4 binding at RP gene promoters was not affected by Sfp1. A-B) ChIP-qPCR reveals the binding of two subunits of NuA4 complex (Epl1 and Eaf1) at the promoter of RPL2B and RPS11B. Sfp1 deleted strains show no significant change compared to the wild-type. Values are a ratio of percentage input. Error bars represent the range of two independent experiments. For ChIP-qPCR of *sfp1* deletion strain, error bars are the standard error of the values (*n*=3). **C)** The Gal-induced Sfp1 overexpression plasmid (HA-tagged Sfp1) was constructed and transformed into the strain expressing myc-tagged. Sfp1 protein levels were determined by western blotting before and after overexpression. Endogenous Myc-tagged Sfp1 shows no protein level change in raffinose and galactose. The Gal-induced Sfp1 overexpression was detected using anti-HA antibody. **D)** ChIP-qPCR indicating Eaf1 binding at RP genes (RPL2B and RPS11B) promoter is not affected upon Sfp1 overexpression. Values are a ratio of percentage input. Error bars represent the range of two independent experiments.

S2 Fig. Heatmaps showing genome-wide histone acetylation changes and Htz1 occupancy change upon Sfp1 depletion. ChIP-seq measured H3K9ac and H4K8ac changes and Htz1 occupancy. An anti-H3 antibody was used to determine total histone occupancy as a control. Signals for a window of -400 to +400 bp relative to TSS were displayed.

S3 Fig. Sfp1 affects histone variant Htz1 occupancy and its acetylation. A) Venn diagram showing the overlap between our wild-type Sfp1 CUT&RUN peaks and published Htz1 ChIP-seq peaks. **B**) Western blot analysis of whole cell extracts from wild-type and *sfp1* deleted cells.

Bulk histone H4 acetylation, Htz1 and Htz1 acetylation levels are shown. Pgk1 signal is shown as loading control.

S4 Fig. K655/657 mutants show almost no effect on Sfp1 protein expression and slight growth defect in YPD. A) Expression of Sfp1 proteins in wild-type and mutated strains. Pgk1 is a reference protein. **B)** The indicated strains were grown to the log phase in YPD. Growth curves were depicted at representative time points.

S5 Fig. Genes involved in metabolic processes were downregulated in Sfp1 K655/657Q strain. Gene set enrichment analysis (GSEA) of RNA-seq data was performed on wild-type cells and acetyl-mimic Sfp1 cells growing in YPD. Top up- and down-regulated pathways are shown.

S6 Fig. Sfp1 regulates RiBi and RP gene expression through different mechanisms upon glucose pulse after carbon source shift. A) RNAs were extracted from log phase wild-type Sfp1, K655/657R, and K655/657Q strains grown in indicated media. Gene expression levels of selected RiBi genes (NSA1 and RPF2) were quantified, relative to levels of *ACT1* mRNA, by RT-qPCR. Values in YPD were normalized to 1. Error bars represent the range of two independent **B)** Volcano plots showing differential gene expression analysis of cells expressing wild-type Sfp1 and K655/657Q mutation. Expression changes at different time points upon glucose pulse after carbon source shift were shown. RP genes were highlighted.

Supplemental Table 1 Yeast strains used in this study.

Strain	Genotype	Reference
LPY3431	*MATa his3Δ200 leu2-3,112 trp1Δ1 ura3-52*	(Clarke et al., Mol Cell Biol 1999)
W303-1A	*MATa ade2-1 his3-11,15 leu2-3,112 can1-100 trp1-1 ura3-1*	(Thomas and Rothstein, Cell 1989)
JKM139	*MATa hoΔ hmlΔ::ADE1 hmrΔ::ADE1 ade1-100 leu2-3,112 trp1::hisG' lys5 ura3-52 ade3::GAL::HO*	(Lee et al., Cell 1998)
QY3530	JKM139 *fpr1Δ*::HphMX *tor1-1::URA3 RPL13A-2*FKBP12::TRP1* (No-FRB)	(Cheng et al., PLoS Genet 2021)
QY3572	Isogenic to QY3530 except FRB-*ESA1*::KanMX	(Cheng et al., PLoS Genet 2021)
QY3810	Isogenic to QY3530 except *SFP1-FRB*::KanMX	this study
QY3811	Isogenic to QY3530 except *SFP1-FRB*::KanMX EPL1-FLAG::NatRMX	
QY3801	LPY3431 *sfp1Δ::KanMX*	this study
QY3802	LPY3431 *SFP1*-MYC::KanMX	this study
QY3803	LPY3431 *SFP1*-MYC::KanMX *EPL1*-FLAG::URA	this study
QY3804	LPY *EPL1*-FLAG::URA	this study
QY3805	LPY3431 *SFP1*-MYC::KanMX + pBG1805(GAL-Sfp1-6*HIS-HA)	this study
QY3806	LPY3431 *SFP1-K655R-K657R-MYC*::KanMX	this study
QY3807	LPY3431 *SFP1-K655Q-K657Q-MYC*::KanMX	this study
QY3808	LPY3431 *SFP1-K655R-K657R*	this study
QY3809	LPY3431 *SFP1-K655Q-K657Q*	this study
YMD070	MATα leu2Δ0 ura3Δ0 his3-1 met15Δ0 sir2Δ::HYGMX hst1Δ::KANMX hst2Δ::HIS3MX	(Rossi et al., Genetics 2016)
QY3812	Isogenic to YMD070 except *SFP1*-MYC::KanMX	this study
QY3813	Isogenic to YMD070 except SFP1- *K655R-K657R-MYC*::KanMX	this study
QY3814	Isogenic to YMD070 except SFP1- *K655Q-K657Q-MYC*::KanMX	this study

S1_Fig

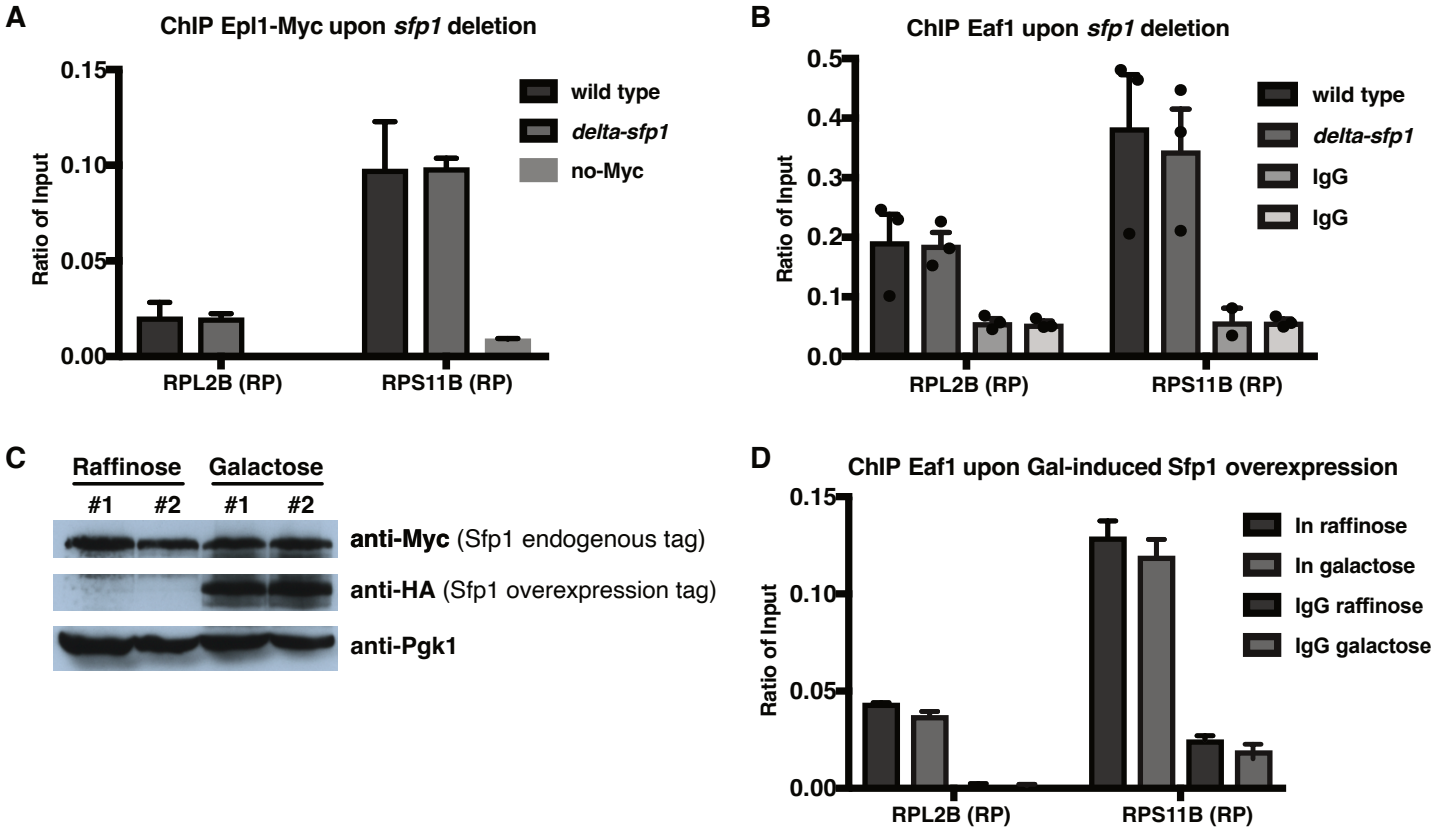
A
ChIP Epl1-Myc upon sfp1 deletion
Ratio of Input
0.15
0.10
0.05
0.00
wild type
delta-sfp1
no-Myc
RPL2B (RP)
RPS11B (RP)
B
ChIP Eaf1 upon sfp1 deletion
Ratio of Input
0.5
0.4
0.3
0.2
0.1
0.0
wild type
delta-sfp1
IgG
IgG
RPL2B (RP)
RPS11B (RP)
C
Raffinose
Galactose
#1
#2
#1
#2
anti-Myc (Sfp1 endogenous tag)
anti-HA (Sfp1 overexpression tag)
anti-Pgk1
D
ChIP Eaf1 upon Gal-induced Sfp1 overexpression
Ratio of Input
0.15
0.10
0.05
0.00
In raffinose
In galactose
IgG raffinose
IgG galactose
RPL2B (RP)
RPS11B (RP)

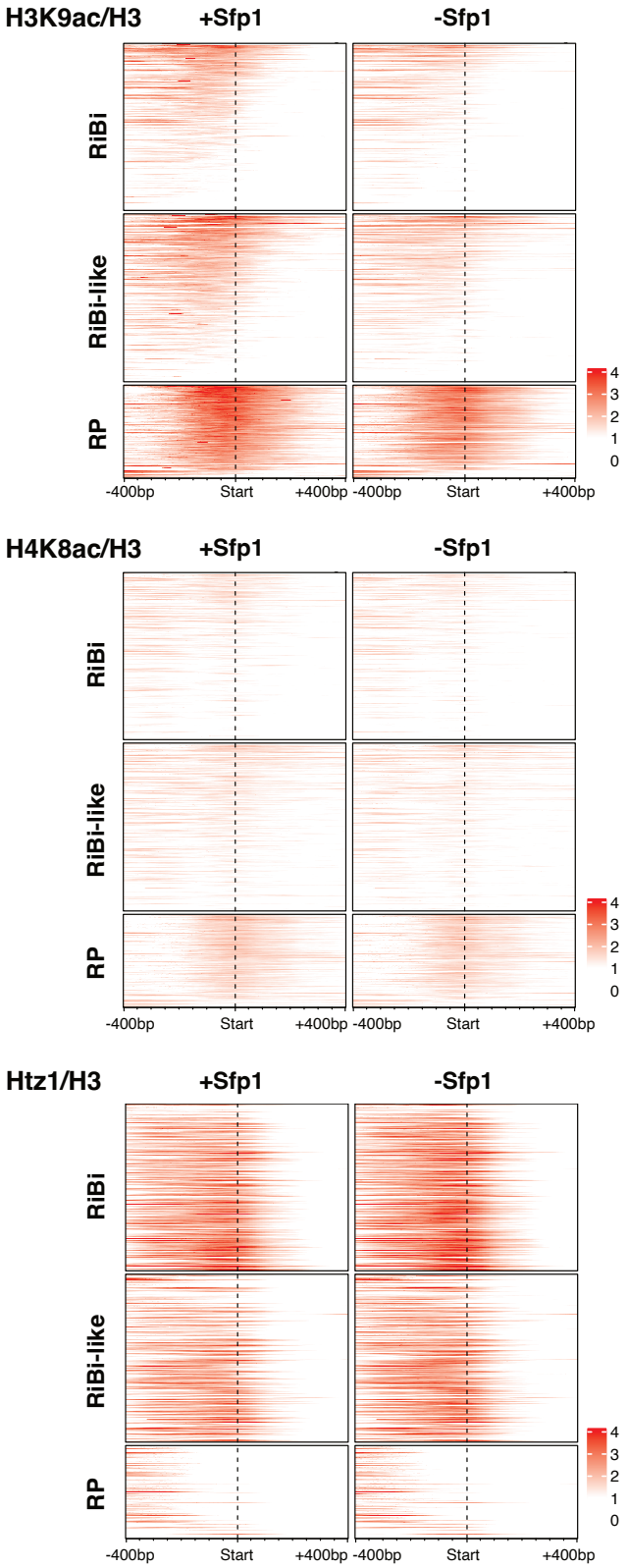
H3K9ac/H3
+Sfp1
-Sfp1
RiBi
RiBi-like
RP
4
3
2
1
0
-400bp
Start
+400bp
-400bp
Start
+400bp
H4K8ac/H3
+Sfp1
-Sfp1
RiBi
RiBi-like
RP
4
3
2
1
0
-400bp
Start
+400bp
-400bp
Start
+400bp
Htz1/H3
+Sfp1
-Sfp1
RiBi
RiBi-like
RP
4
3
2
1
0
-400bp
Start
+400bp
-400bp
Start
+400bp

S3_Fig

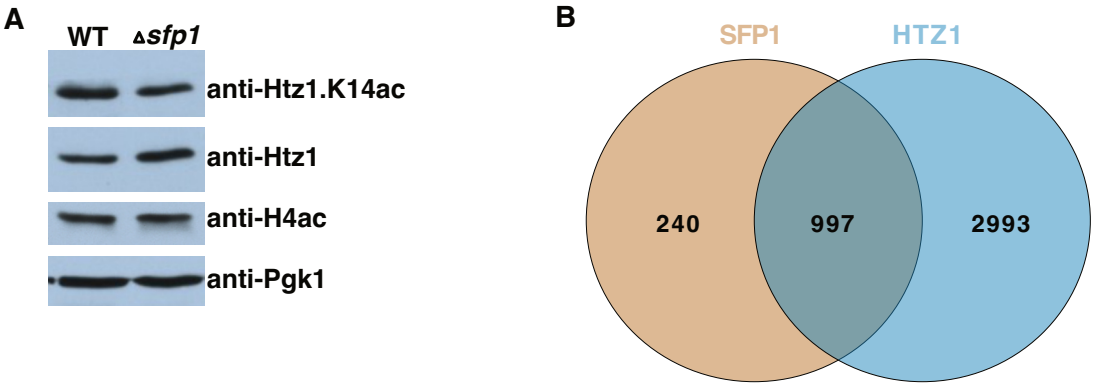
A
WT
Δsfp1
anti-Htz1.K14ac
anti-Htz1
anti-H4ac
anti-Pgk1
B
SFP1
HTZ1
240
997
2993

S4_Fig

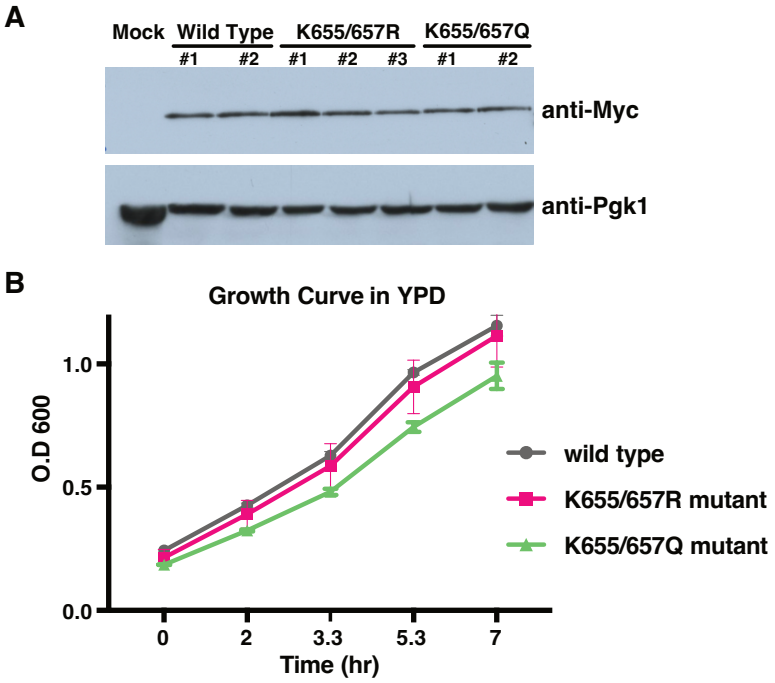
A
Mock
Wild Type
K655/657R
K655/657Q
#1
#2
#1
#2
#3
#1
#2
anti-Myc
anti-Pgk1
B
Growth Curve in YPD
O.D 600
1.0
0.5
0.0
0
2
3.3
5.3
7
Time (hr)
wild type
K655/657R mutant
K655/657Q mutant

S5_Fig

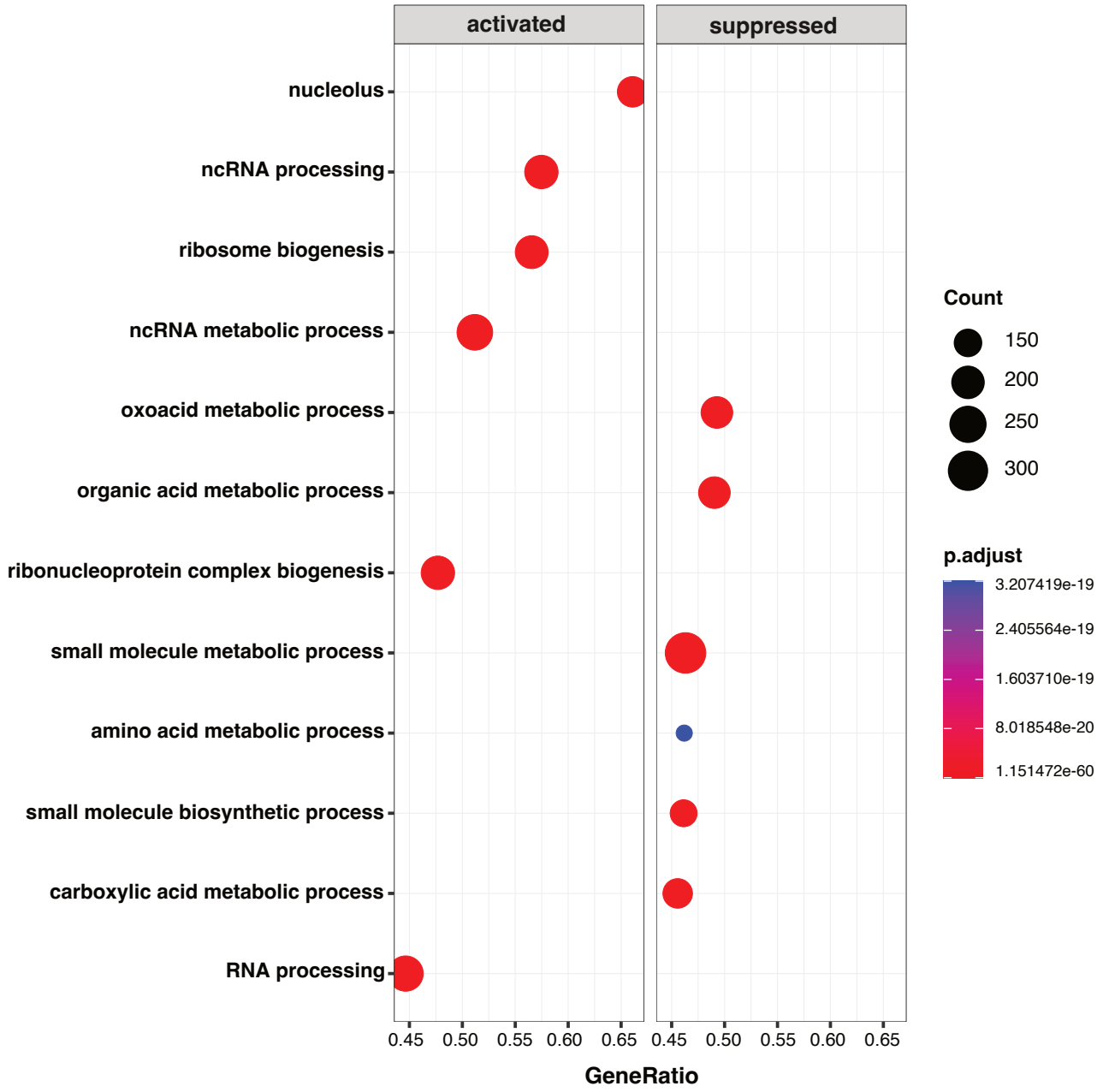
activated
suppressed
nucleolus
ncRNA processing
ribosome biogenesis
ncRNA metabolic process
oxoacid metabolic process
organic acid metabolic process
ribonucleoprotein complex biogenesis
small molecule metabolic process
amino acid metabolic process
small molecule biosynthetic process
carboxylic acid metabolic process
RNA processing
0.45 0.50 0.55 0.60 0.65
GeneRatio
Count
150
200
250
300
p.adjust
3.207419e-19
2.405564e-19
1.603710e-19
8.018548e-20
1.151472e-60

A

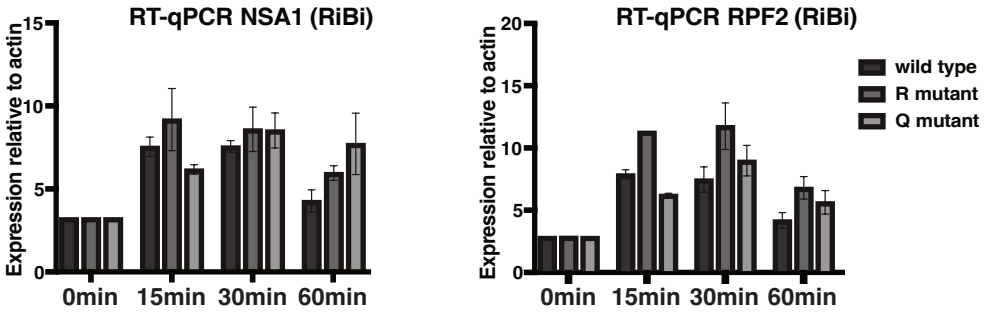
RT-qPCR NSA1 (RiBi)
Expression relative to actin
0
5
10
15
0min
15min
30min
60min
RT-qPCR RPF2 (RiBi)
Expression relative to actin
0
5
10
15
20
0min
15min
30min
60min
wild type
R mutant
Q mutant

B

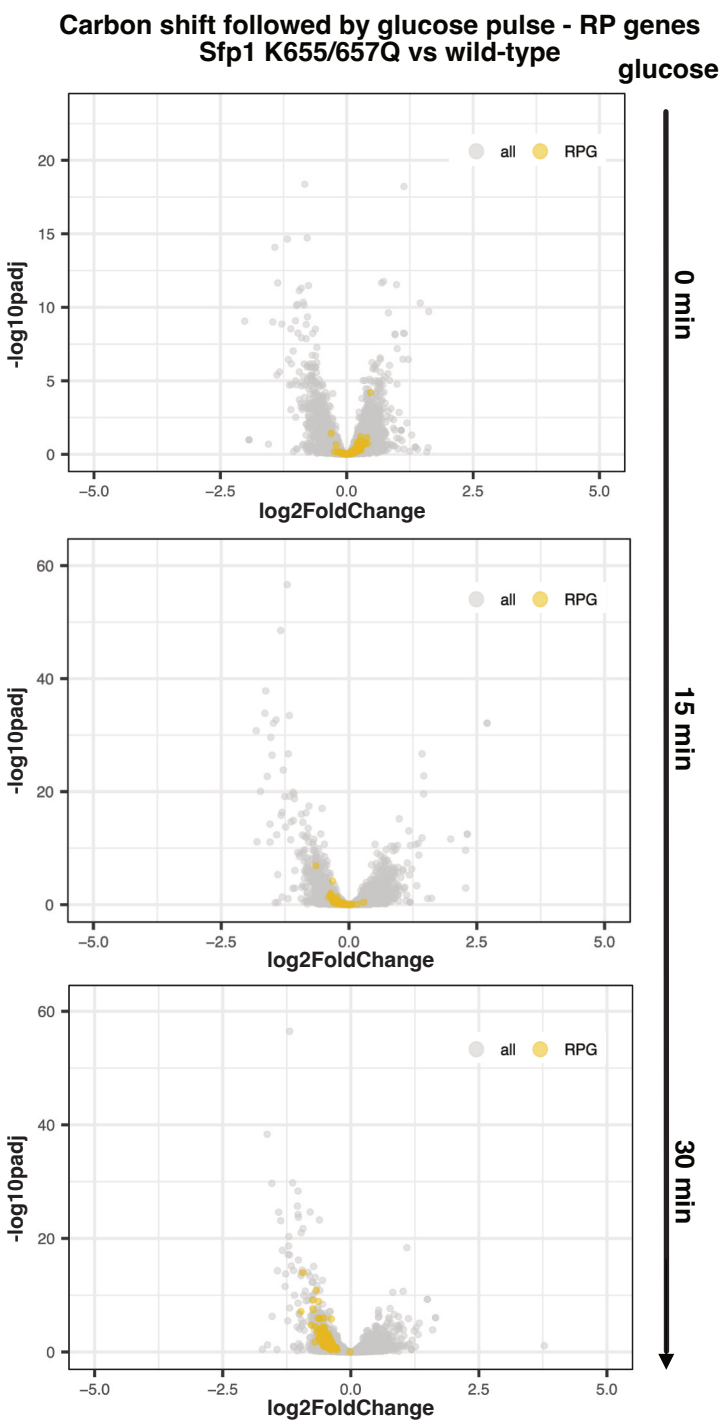
Carbon shift followed by glucose pulse - RP genes
Sfp1 K655/657Q vs wild-type
glucose
0 min
15 min
30 min
all
RPG
-log10padj
log2FoldChange
−5.0
−2.5
0.0
2.5
5.0